Energy dependence of elastic scattering and one-nucleon transfer reactions induced by ^{16}O on ^{208}Pb. I

Steven C. Pieper, M. H. Macfarlane, and D. H. Gloeckner*
Argonne National Laboratory, Argonne, Illinois 60439

D. G. Kovar†
Argonne National Laboratory, Argonne, Illinois 60439
and Lawrence Berkeley Laboratory, University of California, Berkeley, California 94720

F. D. Becchetti,‡ B. G. Harvey, D. L. Hendrie, H. Homeyer,§ J. Mahoney, F. Pühlhofer,‖ W. von Oertzen,§ and M. S. Zisman
Lawrence Berkeley Laboratory, University of California, Berkeley, California 94720
(Received 3 January 1978)

Elastic scattering for ^{16}O on ^{208}Pb and the single-nucleon transfer reactions $^{208}Pb(^{16}O,^{15}N)$ ^{209}Bi and $^{208}Pb(^{16}O,^{17}O)^{207}Pb$ have been measured at bombarding energies of 104, 138.5, and 216.6 MeV. A detailed optical model analysis of ^{16}O on ^{208}Pb elastic data from 80 to 216.6 MeV has been made. The Woods-Saxon potential parameters must be energy dependent to accurately reproduce the elastic data. Finite-range distorted-wave Born-approximation calculations employing both energy- independent and energy-dependent optical potentials are compared with the transfer data. With the exception of small shifts in angle, the distorted-wave Born approximation correctly predicts the shape of the angular distributions and the evolution of the relative single-particle strengths as functions of the bombarding energy. However, the distorted-wave Born approximation fails (by a factor of 2 to 3) to predict the observed energy dependence of the absolute single-particle transfer strength. It is demonstrated that this failure is not likely to be corrected by changes in the bound-state or optical-model potentials, if Woods-Saxon forms that fit the elastic data are used.

[NUCLEAR REACTIONS $^{16}O+^{208}Pb$ elastic, $^{208}Pb(^{16}O,^{15}N)^{209}Bi$, $^{208}Pb(^{16}O,^{17}O)^{207}Pb$, $E_L=104$, 138.5, 216.6 MeV, measured $\sigma(\theta)$; $80 \leq E_L \leq 216.6$ MeV optical-model and distorted-wave Born-approximation analysis, energy dependence of distorted-wave Born approximation.]

I. INTRODUCTION

In this paper data for the elastic scattering of ^{16}O on ^{208}Pb for the single-nucleon transfer reactions ^{208}Pb $(^{16}O,$ $^{15}N)$ ^{209}Bi and ^{208}Pb $(^{16}O,$ $^{17}O)$ ^{207}Pb at ^{16}O bombarding energies of 104, 138.5, and 216.6 MeV are presented. These results are combined with other elastic [1-3] and transfer[4] data in an analysis of the dependence on bombarding energy of ^{16}O-induced single-nucleon transfer reactions on ^{208}Pb from 69.1 to 216.6 MeV. Preliminary discussions of certain aspects of the data presented in this article have been published.[5-7]

Previous studies of heavy-ion transfer reactions have tended to focus on results obtained separately at one or more bombarding energies. Analyses[6,8-14] of single-nucleon transfers induced by ^{11}B, ^{12}C, and ^{16}O ions on ^{208}Pb have led to the conclusion that DWBA adequately reproduces many features of the cross sections of transitions to single-particle and single-hole states for bombarding energies up to 50% above the Coulomb barrier. Systematic differences, however, have been noted[8-11] between the single-neutron pickup and the single-proton stripping reactions. DWBA calculations predict a steady backward shifting of the peaks in angular distributions with increasing excitation energy in the residual nucleus; for the reactions on ^{208}Pb targets, these shifts are present in the neutron pickup data but not in proton stripping. Angle shifts of this sort are found for transfer reactions on a variety of targets across the periodic table. The systematics of the angle shifts and their dependence on Q matching has been discussed[10,15] extensively, but no quantitative interpretation has been given.

The present study covers an energy range from below the Coulomb barrier [E_B (lab) ~ 80 MeV] to $E/E_B \simeq 2.7$. Our DWBA analysis yields results in general agreement with those of earlier studies at the lower end of the energy range; this is discussed in some detail in Sec. VII. The DWBA calculations reproduce the relative intensities of transitions to different single-particle (or single-hole) states with remarkable fidelity at each bombarding energy. A uniform analysis over the complete energy range, however, reveals a new feature: The DWBA cross sections increase more

rapidly with bombarding energy than the measured cross sections. This discrepancy between DWBA and experiment is almost state independent and is present for all the optical potentials—energy dependent and energy independent—considered in this study. It amounts to a factor of about 2.5 over the range of bombarding energies 69.1 to 216.6 MeV (E/E_B from 0.8 to 2.7). Although hints of this gross discrepancy can be detected in earlier studies of single-nucleon transfer reactions on ^{208}Pb, the energy range covered was too small to permit any clear conclusions to be drawn.

The experimental techniques used and the data taken at E_{lab} = 104, 138.5, and 216.6 MeV are discussed in Sec. II. An extensive optical-model analysis of the elastic scattering of ^{16}O from ^{208}Pb at energies from 80 to 216.6 MeV has been carried out; the results of this analysis are presented in Sec. III. A description of the finite-range DWBA with a detailed discussion of the bound-state form factors used is given in Sec. IV. In Sec. V the DWBA angular distributions are compared with experiment and relative spectroscopic factors are extracted. It is shown that DWBA gives accurate predictions of the relative strengths of the transitions at all bombarding energies. Deep minima that occur in the (^{16}O, ^{17}O) reaction are discussed. The energy dependence of the absolute experimental and DWBA cross sections is discussed in Sec. VI. Section VII contains a comparison of this analysis with previous studies of single-nucleon transfers on ^{208}Pb. Section VIII contains a summary of the main conclusions of this study.

II. EXPERIMENTAL TECHNIQUES AND RESULTS

A. Experimental techniques

Elastic scattering of ^{16}O on ^{208}Pb and the single-nucleon transfer reactions ^{208}Pb(^{16}O,^{15}N)^{209}Bi and ^{208}Pb(^{16}O, ^{17}O)^{207}Pb were studied at E_{lab} = 104, 138.5, and 216.6 MeV with beams obtained from the Lawrence Berkeley Laboratory 88-inch cyclotron. Some of the data reported here have already appeared in the literature.[5-7,10] Our final analysis of the data has produced some small modifications in previously reported results; most notably the laboratory energy of the 138.5-MeV data was previously reported as 140 MeV.

Targets of 95% enriched ^{208}Pb of 100–200-μg/cm^2 thicknesses on carbon backings (20 μg/cm^2) were used in all measurements. The outgoing ejectiles were momentum analyzed in the 88-inch cyclotron magnetic spectrometer and detected in a focal-plane detector system previously described in the literature.[16] This detection system measures dE/dx, $B\rho$, and time of flight (TOF) and provides unambiguous particle identification over the momentum range subtended by the detector. Energy resolutions of $\Delta E/E$ = 0.10-0.15% full width at half maximum (FWHM) were obtained in the measurements. Absolute cross sections were established by normalizing the elastic scattering to Rutherford cross sections at forward angles. Relative normalizations were established by use of a monitor at $\theta_{lab} \approx 30°$; these normalizations were consistent with those obtained using the current integrator. The reaction products were generally measured in their highest charge states which were dominant (i.e., $\geq$ 90%) at the energies studied, and charge-state corrections were important only for the lowest energy studied. In the measurements reported here the solid angle was 1 msr or less.

B. Experimental results

The angular distributions measured for the elastic scattering of ^{16}O on ^{208}Pb at E_{lab} = 104, 138.5, and 216.6 MeV are shown in Fig. 1.[17] As mentioned previously the absolute cross sections were established by normalizing the elastic scattering to the Rutherford cross section at forward angles. It is believed that this procedure establishes the cross sections to a precision of at least 10 %. The curves in Fig. 1 represent independent optical-

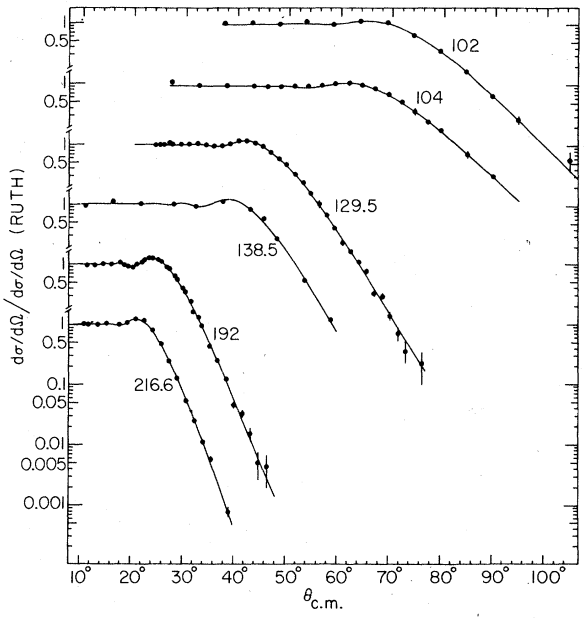

FIG. 1. Elastic differential cross sections for ^{16}O incident on ^{208}Pb. Plotted are the ratios of the cross sections to the corresponding Rutherford cross sections. The curves and data are labeled with the laboratory energy. The solid lines were computed using optical potential *I*3. The 102-MeV data were taken from Refs. 1 and 18 and the 129.5-and 192-MeV data are from Refs. 3 and 19.

model fits to the data at each energy; they are discussed in the next section. Also shown in the figure are elastic scattering data measured at 102 MeV by Videback *et al.*[18] and at 129.5 and 192 MeV by Ball *et al.*[3,19]

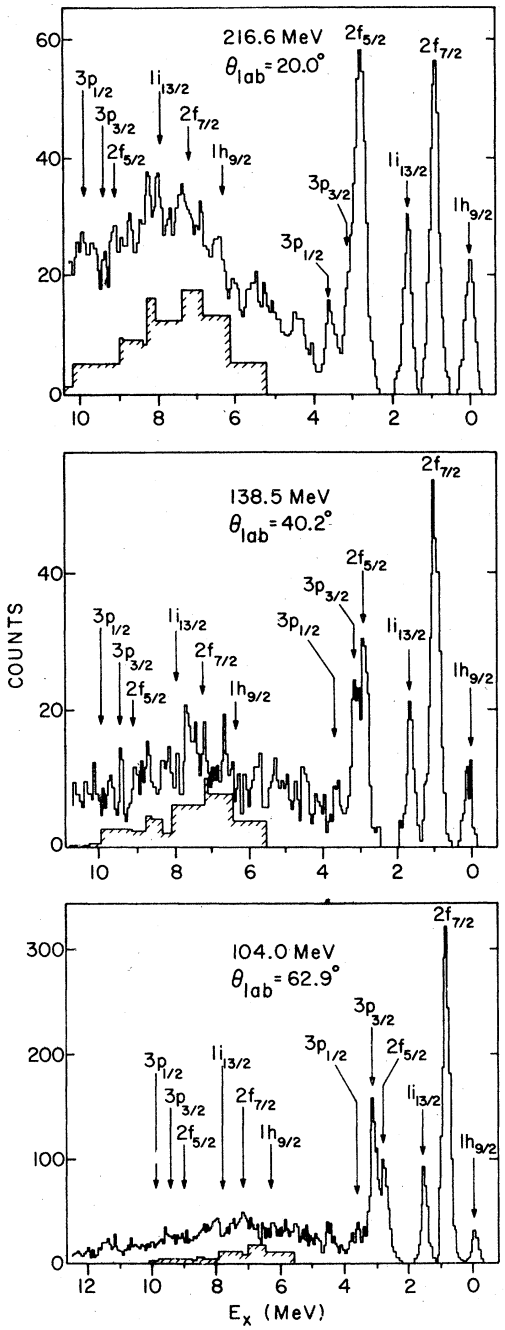

FIG. 2. Spectra for the reactions ^{208}Pb(^{16}O, ^{15}N)^{209}Bi. The arrows show the positions of the indicated single-proton states in ^{209}Bi for ^{15}N left in its ground state ($0 \leq E_x \leq 4$) and in its $1p_{3/2}$ (6.32 MeV) excited state ($6 < E_x < 10$). The shaded histogram is the Doppler broadened DWBA differential cross sections given in Fig. 13.

Energy spectra obtained for the single-proton transfer reaction ^{208}Pb(^{16}O, ^{15}N)^{209}Bi at the three bombarding energies studied are shown in Fig. 2. The angles involved correspond roughly to the angle of maximum transfer cross section for each energy. The six well-known single-proton states in ^{209}Bi (see Fig. 3) are clearly observed. All six single-particle states are unambiguously resolved except for the $2f_{5/2}$, $3p_{3/2}$, and $3p_{1/2}$ states at the higher bombarding energies. At these energies the yields for the three individual states were extracted using a fitting procedure. The angular distributions extracted for the six single-particle states are shown in Fig. 4.[17] The errors associated with the differential cross sections include both statistical and systematic uncertainties and are indicated in Fig. 4. The shaded histograms in Fig. 2 and curves in Fig. 4 are the results of DWBA calculations that are described in Sec. V.

The ^{208}Pb(^{16}O, ^{15}N)^{209}Bi energy spectra obtained at the three bombarding energies show some rather obvious trends. Notably, the strength at excitations greater than 5 MeV is observed to grow significantly with respect to the strength in the resolved single-particle states as the bombarding energy is increased. No obvious peaks can be observed in this region (of higher excitation), and a later discussion will focus on the question of whether the observed strength can be understood as the population of discrete levels. A second observation is that the relative strength of transitions to the various single-particle levels changes rather dramatically as a function of bombarding energy. This energy dependence of the population of levels in ^{209}Bi by the (^{16}O, ^{15}N) reaction has been discussed previously.[6,16] In particular, the results at 104 MeV show a strong preference for the population of $j_>$ ($\equiv l + \frac{1}{2}$) states as opposed to $j_<$ ($\equiv l - \frac{1}{2}$) states

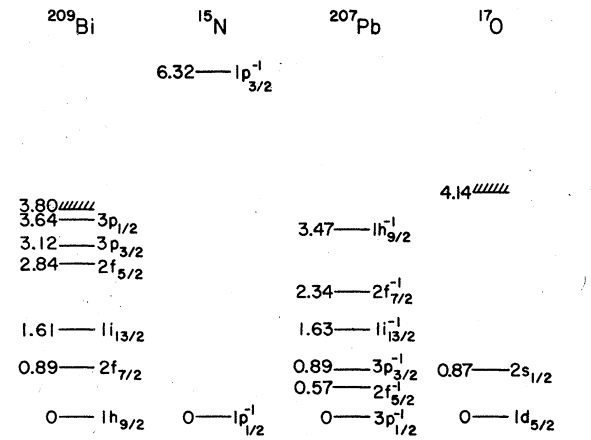

FIG. 3. The single-particle and single-hole states of the nuclei considered in this study.

--a preference that can be understood as a consequence of the selection rules and strong L dependence of the cross section in heavy-ion induced reactions. The present study shows that at higher bombarding energies the preference for spin-flip transitions disappears. The ratio of the peak cross section for the $2f_{7/2}$ state to the peak cross section of the $2f_{5/2}$ state drops from 3 to 0.9 over the range

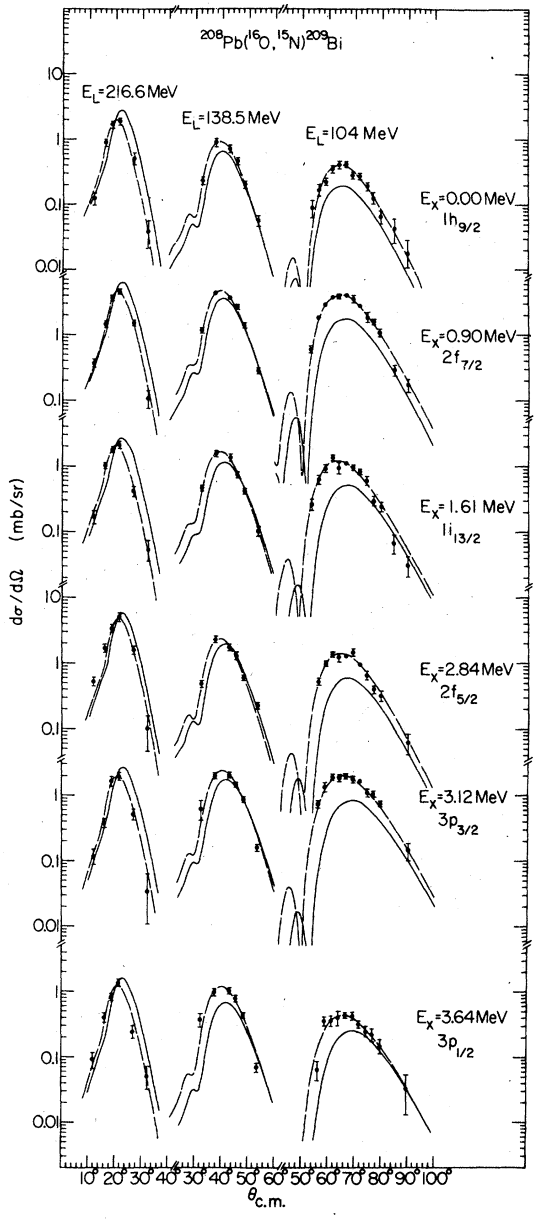

FIG. 4. Differential cross sections for the ^{208}Pb(^{16}O, ^{15}N)^{209}Bi reactions. The solid curves are the results of calculations with optical model *I*3, bound-state potentials O1 and Bi1, and the spectroscopic factors of Table VIII. The dashed curves are those calculations shifted in angle and renormalized to best fit the data.

104 to 216.6 MeV. Similarly the ratio for the two $3p$ states drops from 4.5 to 1.3 (see Fig. 13). The observed behavior is well reproduced by DWBA calculations, as is discussed later.

As a function of bombarding energy, the characteristic bell-shaped angular distributions move to more forward angles and become steadily narrower as the bombarding energy is increased. Moreover, all the angular distributions, at any particular bombarding energy, peak at nearly the same angle independent of excitation energy. Similar features have been noted[9,11,12] in single-proton transfer reactions induced by ^{12}C and ^{11}B ions on ^{208}Pb.

The energy spectra obtained for the single-neutron pickup reaction ^{208}Pb(^{16}O, ^{17}O)^{207}Pb at the three bombarding energies studied are shown in Fig. 5, again at angles that correspond approximately to the peak angle at the appropriate energy. Six groups are observed in the spectra at energies very close to those of the well-known single-neutron hole states in ^{207}Pb (Fig. 3). An identification of the groups with single-hole states cannot, however, be made without further analysis because the excited states of ^{17}O fall into the same region of excitation energies. Figure 6 shows the excitation energies corresponding to transitions leaving ^{17}O in either its ground state or $2s_{1/2}$ excited state and ^{207}Pb in one of its single-neutron hole states. From the figure it is clear that except for the lowest $\frac{1}{2}^-$ and $\frac{5}{2}^-$ states of ^{207}Pb, the groups observed do not involve the population of single levels. Table I shows DWBA calculations of the percentage contribution of each contributing single-particle transition to the groups labeled in Fig. 6. The percentages are based on total transfer cross sections; similar results are obtained for $d\sigma/d\Omega$ in the vicinity of the grazing angle. The table shows that, with the exception of group 4, the cross sections are dominated by transfers leaving ^{17}O in its ground state, although the contributions associated with the $2s_{1/2}$ state of ^{17}O cannot be ignored. At 104 MeV, group 4 could be partially resolved and the data for groups 4a and 4b were also obtained. Extraction of yields for those groups that were not clearly resolved was carried out with a fitting program. The angular distributions obtained are shown in Fig. 7.[17] The errors shown in Fig. 7 include statistical errors and systematic uncertainties resulting from fitting procedures and background subtraction.

The (^{16}O, ^{17}O) energy spectra obtained at the three bombarding energies also show obvious trends. Unlike the (^{16}O, ^{15}N) energy spectra, little strength is observed at higher excitation energies. Like the (^{16}O, ^{15}N) energy spectra, the relative strengths of the various groups populated change

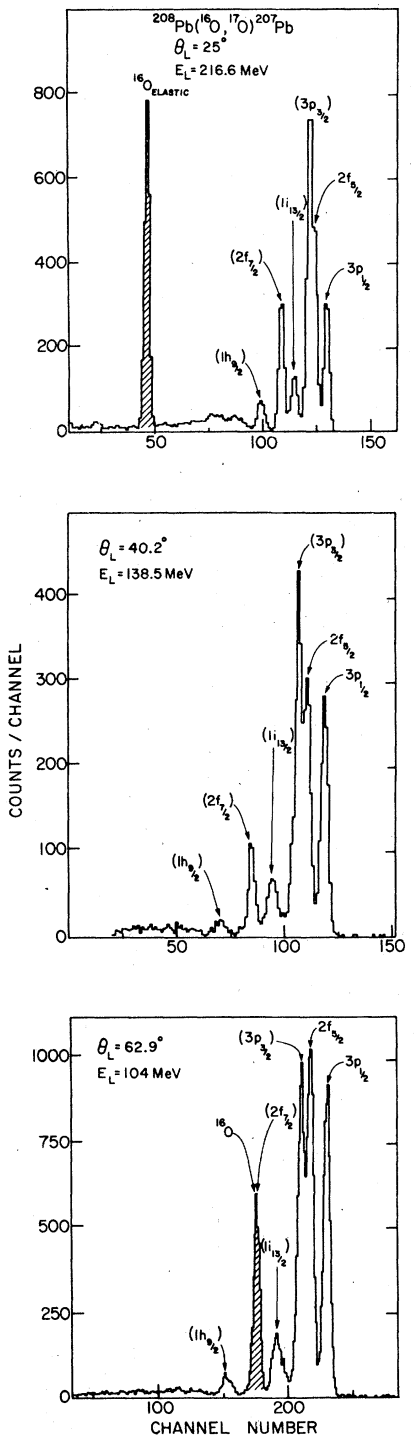

FIG. 5. Spectra for the reactions ^{208}Pb(^{16}O, ^{17}O)^{207}Pb. The arrows show the positions of the single-neutron hole states in ^{207}Pb for ^{17}O left in its ground state. As is discussed in the text, there are also significant contributions from the $2s_{1/2}$ (0.87 MeV) state of ^{17}O. The cross-hatched peak in the 104-MeV spectrum is due to elastic scattering of ^{16}O.

as a function of the bombarding energy. Because of the selection rules for the (^{16}O, ^{17}O) reaction, no strong j dependence in the magnitude of the cross section is expected. Therefore the differences in the selectivity observed in the (^{16}O, ^{17}O) reaction appear to illustrate rather dramatically the effects of kinematic matching on the magnitude of the cross sections.

Total reaction cross sections for each transfer were obtained by integrating the observed angular distributions. Polynomials of various orders were fitted to the data and the resulting functions were then integrated. The data for the (^{16}O, ^{17}O) reactions at 216.6 MeV are fairly sparse for such a procedure, so DWBA differential cross-section curves (shifted in angle and renormalized) were also used as an interpolating device. A weighted average of the values obtained by both methods was then used. The reaction cross sections for (^{16}O, ^{15}N) transfers are given in Table II and those for the (^{16}O, ^{17}O) transfers in Table III.

III. ELASTIC SCATTERING

This section discusses optical-model descriptions of the elastic scattering of ^{16}O on ^{208}Pb at 12 bombarding energies from 80 to 216.6 MeV. In addition to the data at $E_{\rm lab}$ =104, 138.5, and

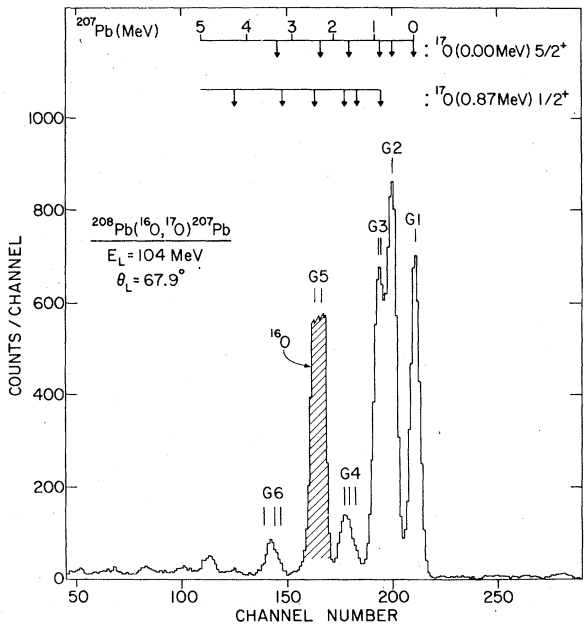

FIG. 6. Spectrum of the reaction ^{208}Pb(^{16}O, ^{17}O)^{207}Pb at $E_{\rm lab}$ = 104 MeV showing the locations of contributions of the single-neutron hole states in ^{207}Pb for ^{17}O left in either its ground state or $2s_{1/2}$ state. The groups discussed in the text are labeled with the letter "*G*" followed by the group number.

TABLE I. Spectral content of the groups observed in the $^{208}Pb(^{16}O,^{17}O)^{207}Pb$ spectra. The percentages are based on DWBA calculations using the spectroscopic factors labeled "present study" in Table X.

Group	State		Excitation	Contribution (%)		
	^{17}O	^{207}Pb	Energy	104 MeV	138.5 MeV	216 MeV
1	$1d_{5/2}$	$3p_{1/2}{}^{-1}$	0	100	100	100
2	$1d_{5/2}$	$2f_{5/2}{}^{-1}$	0.57	100	100	100
3	$2s_{1/2}$	$3p_{1/2}{}^{-1}$	0.87	18	13	8
	$1d_{5/2}$	$3p_{3/2}{}^{-1}$	0.89	82	87	92
4a	$2s_{1/2}$	$2f_{5/2}{}^{-1}$	1.44	31	25	26
4b	$1d_{5/2}$	$1i_{13/2}{}^{-1}$	1.63	13	9	16
	$2s_{1/2}$	$3p_{3/2}{}^{-1}$	1.76	56	66	58
5	$1d_{5/2}$	$2f_{7/2}{}^{-1}$	2.34	99	99	99
	$2s_{1/2}$	$1i_{13/2}{}^{-1}$	2.50	1	1	1
6	$2s_{1/2}$	$2f_{7/2}{}^{-1}$	3.21	19	27	30
	$1d_{5/2}$	$1h_{9/2}{}^{-1}$	3.47	81	73	70

216.6 MeV presented in the previous section this analysis includes ORNL[3,19] data at 129.5 and 192 MeV and BNL data[1,2,18] at seven energies between 80 and 102 MeV. Measurements of elastic scattering at 69.1 MeV[4]—some 10 MeV below the Coulomb barrier—yield cross sections that differ from Rutherford scattering by less than one-half percent at all angles and hence yield no useful information about optical-model parameters.

The character and level of precision of the elastic-scattering analysis in this study are dictated by the fact that the elastic wave functions are to be used in a DWBA analysis of single-nucleon transfer reactions. It is rather well known in this connection that distorted waves generated from optical potentials that yield approximately the same elastic differential cross sections lead to roughly similar DWBA transfer predictions. However, the main conclusion of the transfer analysis in this study is that the energy dependence of the DWBA cross sections is in rather serious disagreement with experiment. It is therefore important to consider the energy-dependence of the optical-model parameters and to show that our main conclusions about the energy dependence of the DWBA transfer cross sections are insensitive to uncertainties in the optical-model parameters and their dependence on energy.

The optical-model fits reported in this section were made with PTOLEMY,[20] an Argonne program for the analysis of heavy-ion-induced direct reactions. A gradient search procedure was used that

TABLE II. Experimental total cross sections for the reaction $^{208}Pb(^{16}O,^{15}N)^{209}Bi$ leaving ^{209}Bi in its single proton states and ^{15}N in its ground state. The errors are based on the differences in the values obtained using various smoothing techniques; they should be increased to 10% to account for possible systematic errors.

State	σ (mb)		
	104 MeV	138.5 MeV	216.6 MeV
$1h_{9/2}$	0.71 ± 0.04	0.76 ± 0.01	0.70 ± 0.05
$2f_{7/2}$	7.36 ± 0.10	3.84 ± 0.05	1.68 ± 0.05
$1i_{13/2}$	2.14 ± 0.05	1.39 ± 0.03	0.74 ± 0.02
$2f_{5/2}$	2.50 ± 0.05	1.94 ± 0.05	1.83 ± 0.05
$3p_{3/2}$	3.85 ± 0.02	2.06 ± 0.05	0.68 ± 0.02
$3p_{1/2}$	0.85 ± 0.05	1.08 ± 0.02	0.44 ± 0.05

TABLE III. Experimental total cross sections for the groups observed in the spectra of the $^{208}Pb(^{16}O,^{17}O)^{207}Pb$ reaction. See Table II for the significance of the error estimates.

Group	σ (mb) at		
	104 MeV	138.5 MeV	216.6 MeV
1	23.2 ± 1.0	19.6 ± 0.5	8 ± 2
2	27.1 ± 0.5	19.1 ± 0.5	9.0 ± 0.2
3	23.0 ± 1.0	30.1 ± 0.5	23 ± 1
4	8.0 ± 0.2	8.08 ± 0.10	4.5 ± 0.2
4a	2.5 ± 0.3	...	...
4b	5.5 ± 0.2	...	...
5	...	8.7 ± 0.3	8 ± 1
6	3.95 ± 0.10	4.8 ± 0.1	2.6 ± 0.3

makes specific use of the sum of squares character of the function to be minimized. The necessary gradients were computed from an integral over the scattering wave functions rather than by difference techniques. Reference 21 contains a detailed description of the optical-model fitting techniques employed.

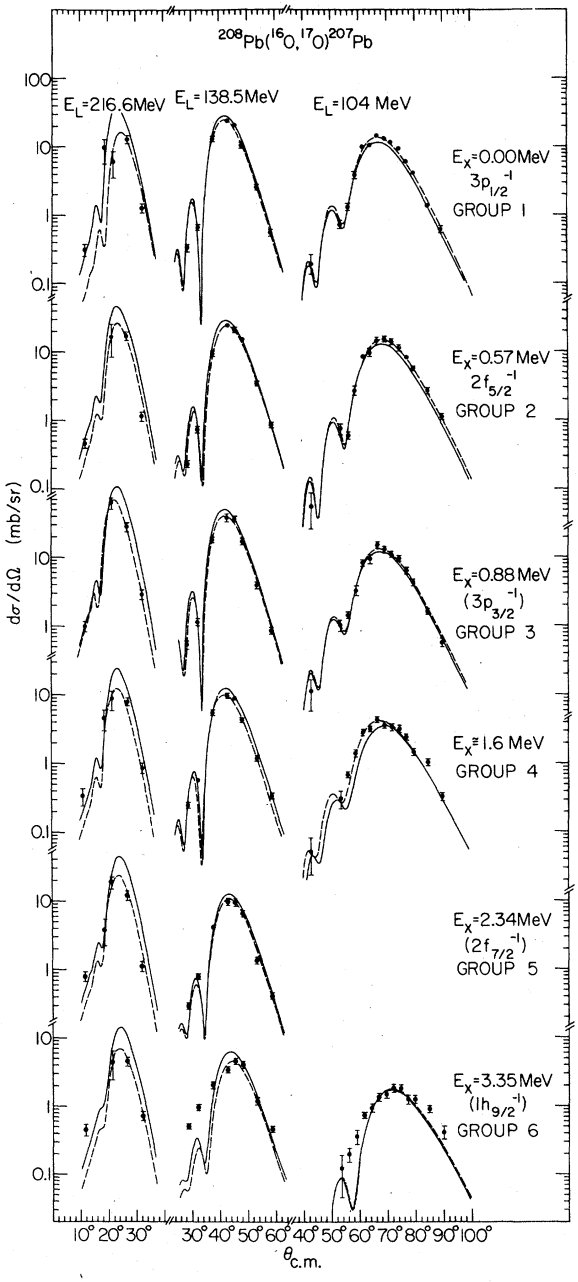

FIG. 7. Differential cross sections for the ^{208}Pb(^{16}O, ^{17}O)^{207}Pb reactions. The curves and data are labeled with the group numbers of Table I. The solid lines were computed using optical potential *I*3, bound-state potentials O1 and Pb1, and the spectroscopic factors of Table X. The dashed curves are these calculations shifted in angle and renormalized to best fit the data.

A. Potential forms

The optical potentials used in this work consist of the Coulomb potential between a point charge and a uniformly charged sphere and of Woods-Saxon forms for the real and imaginary nuclear potentials:

$$U(r) = U_C(r) + U_N(r) , \tag{3.1}$$

where

$$U_C(r) = \begin{cases} \dfrac{Z_p Z_t e^2}{2R_C}\left[3 - \left(\dfrac{r}{R_C}\right)^2\right], & r < R_C , \\ \dfrac{Z_p Z_t e^2}{r} , & r \geq R_C , \end{cases} \tag{3.2}$$

$$U_N(r) = -V_r f(r, R_r, a_r) - i V_i f(r, R_i, a_i) , \tag{3.3}$$

and

$$f(r, R, a) = \{1 + \exp[(r - R)/a]\}^{-1} \tag{3.4}$$

is the Woods-Saxon radial function; $Z_p e$ and $Z_t e$ are the charges of the projectile and the target. The potential radii (R_C, R_r, and R_i) are related to radius parameters (r_C, r_r, r_i) by

$$R_x = r_x (A_p^{1/3} + A_t^{1/3}) , \tag{3.5}$$

where A_p and A_t are the atomic weight of the projectile and target. Potentials with surface absorption were also considered. The transfer results obtained with such potentials do not differ significantly from those obtained with volume absorption; accordingly, volume absorption is assumed throughout. The Coulomb radius parameter was fixed at $r_C = 1.3$ fm for all the potentials reported here. We have found that the use of the Coulomb potential between two uniformly charged spheres gives results for both elastic scattering and transfer that differ by less than 1% from those obtained with the simpler potential of Eq. (3.2).

B. Individual-energy fits

The most straightforward method of constructing optical potentials that reproduce elastic data taken at a variety of bombarding energies is to make individual fits at each energy. Six-parameter fits in which the depth, radius, and diffuseness of the real and imaginary parts of the potential are varied have been made. Analysis of the eigenvalues of the 6 × 6 relative covariance (or error) matrix for such fits reveals that the ^{16}O + ^{208}Pb elastic

data do not contain enough information to determine all six parameters; e.g. there are two linear combinations of parameters that are determined to better than 1%, one determined to within 2 to 10%, one determined to within 20 to 50%, and two linear combinations of parameters totally undetermined by the data. The poorly determined eigenvectors are dominated by the potential depths. Two main qualitative conclusions emerge from this error-matrix analysis:

(1) The elastic data presented in the previous section determine only three or four parameters of the potential at each energy.

(2) The geometrical parameters should be varied rather than the depths since the data are relatively insensitive to variations in the depths.

Two-, three-, and four-parameter fits in which the well depths are fixed at $V_r = V_i = 50$ MeV have been made at each energy. In the two-parameter fits (referred to as *I*2) the real and imaginary geometric parameters are constrained to be equal so that $r_r = r_i$ and $a_r = a_i$ are varied. The three-parameter fits (*I* 3) have distinct real and imaginary radii with $a_r = a_i$. Finally in the four-parameter fits (*I* 4) all four geometric parameters are separately varied.

Since the experimental errors in the elastic data include estimates of systematic errors, it is not to be expected that a value of χ^2 per data point around unity is a reliable signature of a good fit. Indeed for several of the elastic data sets three- or four-parameter fits yield values of 0.05 to 0.1 for χ^2 per point. We therefore choose the ratio of χ^2 to that for the four-parameter fit *I*4 as the figure of merit for our elastic fits. The value of χ^2 improves significantly in going from two- to three-parameter fits; the step from three- to four-parameter fits yields a much smaller reduction in χ^2. At the same time, the best fit parameters in the two-parameter fits vary rather smoothly with energy; this smoothness survives in the three-parameter fits but the four-parameter fits yield parameters that fluctuate considerably from one bombarding energy to the next. These properties of the energy dependence are shown for the real diffuseness parameter in Fig. 8; similar results are obtained for the other geometrical parameters.

Our study of two-, three-, and four-parameter fits thus confirms the results of the error-matrix analysis—the elastic data fix no more than three parameters of the potential at each energy. We therefore use the three-parameter fit *I*3 as our standard individual-energy optical-model parameterization. The parameters of fit *I*3 are given in Table IV at the bombarding energies for which DWBA calculations were made. The calculated angular distributions are shown in Fig. 9 to be in excellent agreement with experiment.

Variation of other parameter combinations were also investigated. Potentials were obtained from fits in which the geometric parameters are fixed and V_r and V_i are allowed to vary. One such fit (*I*2′) is obtained by setting $r_r = 1.2$, $r_i = 1.22$, $a_r = a_i = 0.615$. The resulting well depths are shown in Fig. 10. The values of χ^2 are significantly larger than those obtained when two geometrical parameters are varied (fit *I*2). This is not surprising since, as was shown in the discussion of the eigenvalues of the error matrix, the well depths are the most poorly determined potential parameters.

Many other individual-energy fits were made in which different combinations of parameters (e.g., $r_r = r_i$, a_r, or V_r, V_i, and $a_r = a_i$) were varied or in which parameters that are not varied are fixed at different values (e.g., geometric parameters varied for $V_r = 100$, $V_i = 20$, or $V_r = V_i = 30$). The results are always similar to those presented above: The data seem to require three parameters, and most three-parameter fits give a good representation of the data (provided of course that the geometrical rather than the depth parameters are varied).

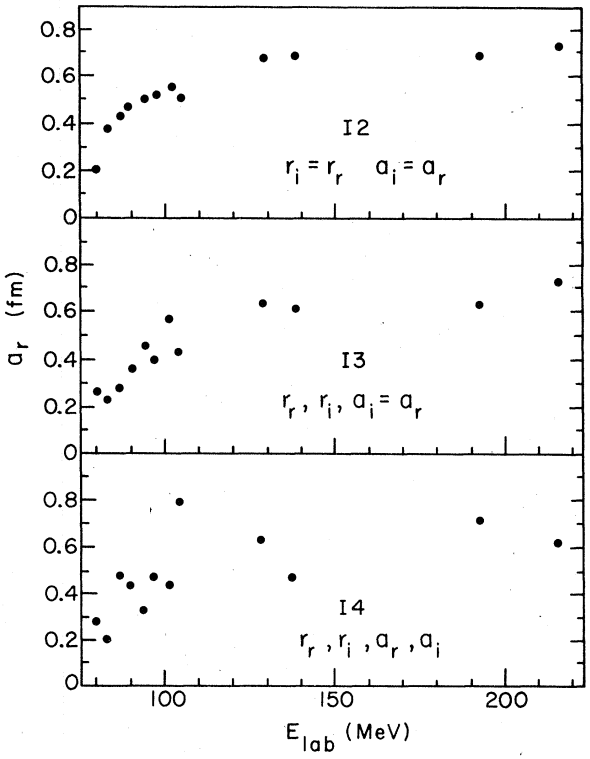

FIG. 8. The real diffuseness parameter, a_r, as a function of bombarding energy for the independent-energy fits *I*2, *I*3, and *I*4.

TABLE IV. Optical potential parameter values for the entrance channel for the bombarding energies at which DWBA calculations were made. As is explained in the text, the exit parameters are slightly different in all cases except potential *I3*. See Table V for potential *C*. Potential depths are in MeV, radii and diffusenesses in fm.

Potential	Parameter	104 MeV	138.5 MeV	216.6 MeV
I3	$V_r = V_i$	50	50	50
	r_r	1.317	1.221	1.133
	r_i	1.293	1.194	1.135
	$a_r = a_i$	0.419	0.612	0.736
L	V_r	98.91	73.78	16.86
	V_i	23.00	18.53	8.31
	r_r	1.175	1.203	1.264
	r_i	1.258	1.285	1.346
	$a_r = a_i$	0.605	0.603	0.599
Q	V_r	51.09	51.09	51.09
	V_i	51.46	51.46	51.46
	$r_r = r_i$	1.281	1.210	1.145
	a_r	0.498	0.676	0.706
	a_i	0.429	0.625	0.708

C. Fits with smooth energy dependence

Figure 8 shows that even the two- and three-parameter, fixed-depth fits yield parameters whose energy dependence gives some indication of erratic excursions from one energy to the next. In an attempt to produce potentials with a smooth behavior with energy, we have made multiple-energy optical-model fits. For these fits, the potential parameters were taken to have either no energy dependence or one or more of the potential parameters were given a linear or quadratic dependence on the bombarding energy.

The simplest such potentials are those in which all parameters are energy independent; they yield uniformly poor fits to the data. An example is fit *C* which is fitted to the data from 96 to 216.6 MeV. The well depths are fixed at $V_r = 100$ MeV and $V_i = 24$ MeV while the four geometric parameters are varied. The resulting parameters are given in Table V and the predicted cross sections are compared to the elastic data in Fig. 9. It is clear that the fit to the data is much poorer at some energies than was obtained with the individual-energy fits. The quality is not significantly improved by choosing values of the depth parameters different from those used in potential *C* nor by permitting all six potential parameters to vary.

TABLE V. Parameters of the optical potentials with a smooth energy dependence. Given are the coefficients α, β, and γ of quadratic expansions for the parameters: parameter $= \alpha + \beta E_{\text{lab}} + \gamma E_{\text{lab}}^2$. Values marked with an asterisk were not varied during the search; coefficients that are zero were also not varied. Potential depths are in MeV, radii and diffusenesses in fm.

Potential	Parameter	α	β	γ
C	V_r	100*	0	0
	V_i	20*	0	0
	r_r	1.090	0	0
	r_i	1.273	0	0
	a_r	0.777	0	0
	a_i	0.597	0	0
L	V_r	174.7	−0.729	0
	V_i	36.6	−0.1305	0
	r_r	1.093	0.792×10^{-3}	0
	r_i	1.176	0.785×10^{-3}	0
	$a_r = a_i$	0.610	-0.51×10^{-4}	0
Q	V_r	51.09	0	0
	V_i	51.46	0	0
	$r_r = r_i$	1.653	-0.471×10^{-2}	0.109×10^{-4}
	a_r	−0.651	0.01546	-0.425×10^{-4}
	a_i	−0.629	0.01416	-0.369×10^{-4}

The poor agreement with experiment obtained with fit C seems to be characteristic of all energy-independent fits to the $^{16}O+^{208}Pb$ data.

Recently Cramer *et al.*[22] have reported a shallow energy-independent potential for elastic $^{16}O+^{28}Si$ elastic scattering over a large energy range. Satchler[23] has demonstrated that deeper folded potentials will give comparable fits if one of the parameters (i.e., a_i) is given a linear dependence on the bombarding energy. However, the quality of the fits in both cases is quite poor at the intermediate energies at which the data have pronounced oscillations at large angles while the potential produces a smooth falloff. Individual fits of Woods-Saxon potentials are capable of producing oscillations that significantly improve the fit at these energies; however, the χ^2 per point is still about 5. We regard our energy-independent

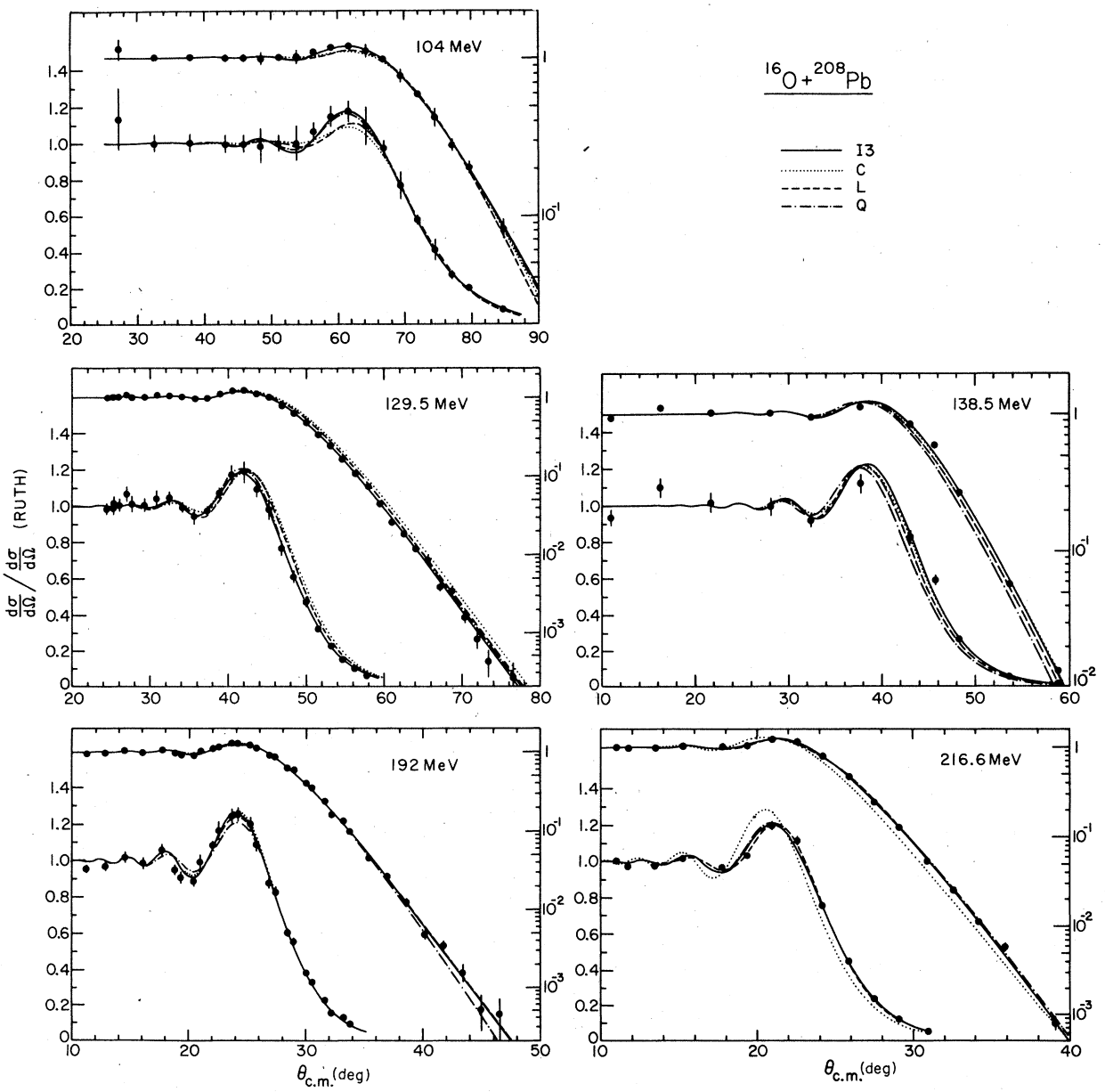

FIG. 9. Elastic differential cross sections for ^{16}O on ^{208}Pb at bombarding energies of 104 to 216.6 MeV. The top set of curves and data corresponds to the logarithmic scale on the right; the lower set corresponds to the linear scale on the left. The curves show optical-model predictions for the four indicated potentials.

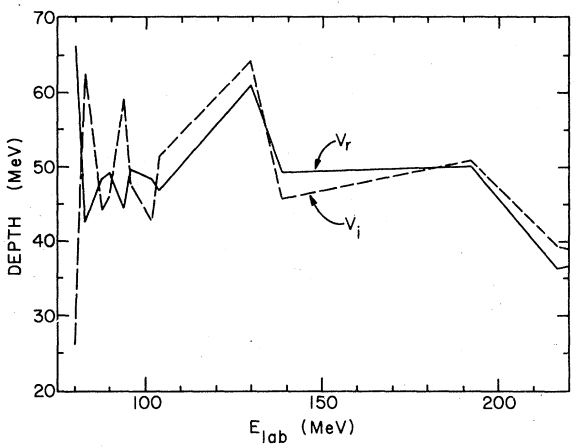

FIG. 10. Well depths for potential *I2'*.

potentials as inadequate representations of the elastic data; the data for the $^{16}O+^{208}Pb$ system appear to demand an energy dependence in the parameters of optical-model potentials of Woods-Saxon form.

A number of potentials were considered in which one or more parameters has a linear energy dependence. Such potentials consistently fail at one or more energies. Potential *L*, a 10-parameter fit, is typical; its parameters are listed in Table V. The predicted cross sections are compared with the elastic-scattering data in Fig. 10; it is clear that the fit at 104 MeV is quite poor while the fits at higher energies are better. The χ^2 values at most energies are substantially poorer than those obtained in the individual-energy fits.

Many fits were made in which one or more of the parameters are given a quadratic energy dependence. These were generally limited to the data from 104 to 216.6 MeV. It was found that 12 parameters are the most that this data can support. In the various fits different combinations of parameters were given quadratic energy dependence and different weights were assigned to the data taken at the five energies between 104 and 216.6 MeV. The use of different weights yields better or poorer fits at specific energies, but no fit was found that accurately reproduces the data at all five energies from 104 to 216.6 MeV. Potential *Q* is a typical example that was obtained in an 11-parameter fit in which the well depths are independent of bombarding energy and quadratic energy dependences are allowed for $r_r = r_i$, a_r, and a_i. The parameters of this potential are given in Table V, and the predicted cross sections are compared with experiment in Fig. 9. Assessed relative to the individual-energy fit *I3*, it is clear that the quadratic form for the smoothed energy dependence has resulted in marked degradation of the quality of the fits.

Potentials that are functions of E_{lab}^{-1} might be expected to give a better representation of the data since they could have reasonable high-energy extrapolations. A number of attempts were made to produce potentials whose parameters depended quadratically on E_{lab}^{-1}, however, the results were very similar to those reported above and the potentials generally do not extrapolate well to high energies.

In summary, we have attempted to find optical potentials for the $^{16}O+^{208}Pb$ data that depend smoothly on bombarding energy. Constant, linear, and quadratic dependence on E_{lab} or E_{lab}^{-1} yield potentials that fit the data much more poorly than do the individual-energy parametrizations discussed in Sec. III B.

D. Total reaction cross sections

The discussion in the preceding section focuses on the quality of the fits obtained to the elastic scattering data with various optical-model parametrizations. The lowest values of χ^2 were obtained in the individual-energy fits. All parametrizations which demand a smooth energy dependence of parameters resulted in poorer fits.

Figure 11 shows the total reaction cross sections predicted by a number of the potentials discussed above. It is clear that the reaction cross sections of the individual-energy fits fluctuate about those of the smoothly varying potentials. A particularly noticeable discontinuity occurs in the 130- to 140-MeV range. This can also be seen in Fig. 9: Potential *Q* gives an excellent representation of the 129.5-MeV data but yields cross sections significantly too small at 138.5 MeV. On

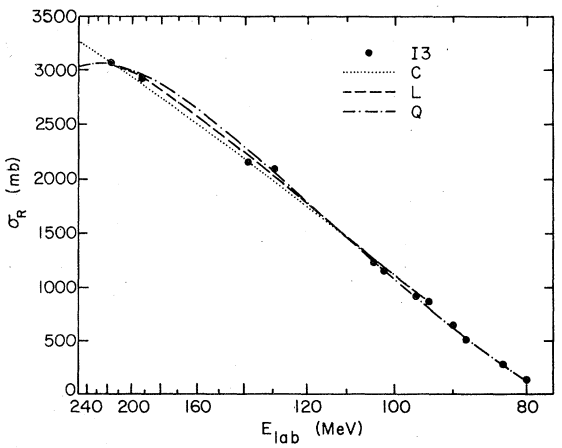

FIG. 11. Total reaction cross sections for $^{16}O+^{208}Pb$ computed using several of the optical potentials discussed in the text. The abscissa is $1/E_{c.m.}$.

the other hand, potential C fits the 138.5-MeV data well but yields cross sections that are too large at 129.5 MeV. Also Fig. 10 shows that the 129.5 data require well depths significantly out of line with those indicated by the rest of the data. It will require more data in this energy range to determine if this apparent discontinuity is real or is due to a systematic error in one or both sets of data. In this regard it should be noted that the 138.5-MeV data are consistent with new 138.5-MeV elastic data that were also obtained on the Berkeley 88-inch cyclotron.[24]

IV. DWBA CALCULATIONS

Finite-range DWBA calculations for the ^{208}Pb(^{16}O, ^{15}N)^{209}Bi and ^{208}Pb(^{16}O, ^{17}O)^{207}Pb single-nucleon transfer reactions were performed with the program PTOLEMY.[20] Most of the ingredients of the calculations are quite standard and are described, for example, in Refs. 9–11 and 25.

A. Optical-model parameters

The distorted waves were those obtained from the elastic fits presented in Sec. III. Exit channel optical-model parameters were taken to be the same as those in the entrance channel. (In the energy-dependent parameter sets, the energy was, of course, adjusted for the Q value.) Such a choice for the exit channels appears to be justified by the results of other studies. In Ref. 11 the elastic scattering in both entrance and exit channels was measured for the reactions ^{208}Pb(^{12}C, ^{13}C)^{207}Pb and ^{208}Pb(^{12}C, ^{11}B)^{209}Bi; DWBA predictions using optical-model potentials separately fitted to the entrance- and exit-channel data were not significantly different from those obtained using entrance-channel optical-model parameters in both channels. Similar results were obtained in a study[26] of ^{16}O-induced reactions on isotopes of Ca.

Extensive studies were undertaken of the dependence on the optical-model parameters of the DWBA cross sections for the transfer reactions ^{208}Pb(^{16}O, ^{15}N)^{209}Bi and ^{208}Pb(^{16}O, ^{17}O)^{207}Pb. We will concentrate here on the results obtained with the four representative potentials introduced in Sec. III—*I*3 (individual-energy fit), *C* (energy-independent potential), *L* (potential with parameters linearly dependent on energy), and *Q* (quadratic energy dependence). The parameters of these potentials at $E_{\rm lab}$ = 104, 138.5, and 216.6 MeV are given in Table IV; the energy-dependent expressions for the parameters of potentials *C*, *L*, and *Q* are given in Table V. Since these potentials do not predict the same elastic scattering they might be expected to give somewhat different DWBA transfer results. However, the absolute values of the cross sections in the vicinity of the peak generally differ by less than 20%. The cases where more significant differences are observed are (e.g. potentials *C* and *L* at 104 MeV) are correlated with the inability of the smooth potentials to accurately reproduce the corresponding elastic scattering.

We find, as in previous studies,[26] that potentials that give nearly identical predictions for elastic scattering also predict very nearly the same DWBA cross sections in the angular range of interest in the present study. In other words, the elastic-scattering data fix the distorted waves in the near-grazing partial waves closely enough to leave little leeway in the DWBA cross sections.

B. Effective interaction

The effective transition operator in the DWBA calculations was taken to be the light-ion binding potential with the Coulomb and core-Coulomb corrections discussed by DeVries *et al.*[25] These corrections decrease absolute cross sections for the proton-stripping reaction by about 25% and increase the neutron pickup cross sections by a few percent; in both cases they bring the post and prior versions of DWBA into agreement at the 2 or 3% level. A few calculations were also made including the core corrections for the real part of the nuclear optical potentials; these corrections were found to change the cross sections by no more that 3%. Toth *et al.*[11] find that the core corrections for the imaginary part of the optical potential have an even smaller effect on the cross sections. Thus, DWBA calculations that include only the Coulomb part of the core corrections to the effective transition operator should be accurate at the 2 to 3% level—about the size of the residual post-prior discrepancy.

C. Bound-state wave functions

The bound-state form factors used assume that ^{16}O and ^{208}Pb are good enough closed-shell nuclei that the relevant states of ^{15}N, ^{17}O, ^{207}Pb, and ^{209}Bi can be described as single-hole or single-particle states. The form factors are then radial Woods-Saxon wave functions multiplied by spectroscopic amplitudes designed to allow for small departures from the extreme single-particle model.

The bound-state potentials used have Coulomb and real Woods-Saxon terms of the form given in Eqs. (3.2) and (3.3) with a real spin-orbit component:

$$v_{so} = 4V_{so}\, L \cdot S\, \frac{1}{r}\, \frac{df(V_{so}, R_{so}, a_{so})}{dr} . \qquad (4.1)$$

where f is the Woods-Saxon radial function [Eq.

TABLE VI. Parameters of the bound-state potentials. Unless otherwise stated, the first three potentials have been used for all figures and tables; the remaining potentials were used only to study the sensitivity of the DWBA cross sections to the bound-state potentials.

Designation	System	V_r [a] (MeV)	r_{or} (fm)	a_r (fm)	V_{so} [b] (MeV)	r_{so} (fm)	a_{so} (fm)	r_C (fm)	Ref.
O1	$^{16}O_{-p}^{+n}$	56.5 62.5	1.2	0.65	7	1.2	0.65	1.2	10
Bi1	$^{208}Pb+p$	60	1.28	0.76	6	1.09	0.6	1.2	9
Pb1	$^{208}Pb-n$	45.6	1.25	0.63	7	1.1	0.5	···	9
Bi2	$^{208}Pb+p$	60	1.24	0.65	$\lambda=6$	1.24	0.65	1.25	29
Pb2	$^{208}Pb-n$	40.5	1.36	0.73	7.07	1.26	0.6	···	27
Pb3	$^{208}Pb-n$	45.5	1.25	0.63	$\lambda=27.5$	1.25	0.63	···	28

[a] V_r is adjusted for each state to reproduce the experimental separation energies. The median value is given.

[b] When a value for λ is given, $V_{so}=\frac{1}{4}\lambda V_r/45.2$, and is different for each state.

(3.4)]. For the bound-state potentials, radii are related to radius parameters by

$$R_x = r_x A_c^{1/3}, \tag{4.2}$$

where A_c is the atomic weight of the core.

The potential parameters chosen for nucleons bound in the heavy nuclei were those used in Ref. 9 and are given in Table VI (Bi1 and Pb1). For nucleons bound in the lighter nucleus the light-ion binding potential of Ref. 10 was adopted (O1 in Table VI). Following the conventional separation energy prescription, the depths of the real potentials were adjusted to reproduce the observed separation energies; the state-to-state variation in potential depth introduced in this way is less than 1.5% for the ^{209}Bi states and less than 5% for the ^{207}Pb states.

1. ^{209}Bi bound-state wave functions

The potential Bi1 used here and in Ref. 9 for the single-particle levels in ^{209}Bi yields reasonable agreement[27] with experiment for the spectrum of ^{209}Bi, for the rms charge radius of ^{208}Pb, and for the elastic scattering of 175- and 250-MeV electrons from ^{208}Pb. Despite these constraints, small variations in the parameters of the potential are not ruled out by existing data. Previous studies[9,28] have shown that such small variations can result in large changes in the predicted cross sections. Table VII compares cross sections obtained using the somewhat different potential Bi2, which has been used to analyze ^{208}Pb(^{3}He, d)^{209}Bi data,[29] to those computed with potential Bi1. Since Ford *et al.*[9] reanalyzed the data of Ref. 29 with potential Bi1, we can also assess the influence of this change

TABLE VII. Sensitivity of the (^{16}O,^{15}N) DWBA cross section to the ^{208}Pb + p bound-state potential. Shown are the ratios of the DWBA total transfer cross sections computed using potential Bi1(σ_j) and Bi2(σ_j'). Also shown are ratios for the ^{208}Pb(^{3}He,d)^{209}Bi reaction at 51.3 MeV using the same potentials. These ratios are based on the spectroscopic factors given in Refs. 29 and 9. The squared ratios of the bound-state wave function are also given.

State in ^{209}Pb	σ_j/σ_j'				$(\phi_j/\phi_j')^2$	
	(^{16}O, ^{15}N)			(^{3}He,d)	10 fm	∞
	104 MeV	138.5 MeV	216.6 MeV	51.3		
$1h_{9/2}$	2.11	2.09	2.03	1.85	2.09	2.17
$2f_{7/2}$	1.93	1.89	1.83	1.72	1.88	1.96
$1i_{13/2}$	···	···	···	1.81	2.10	2.17
$2f_{5/2}$	2.11	2.08	2.02	1.87	2.06	2.15
$3p_{3/2}$	1.88	1.82	1.76	1.86	1.83	1.91
$3p_{1/2}$	1.93	1.91	1.83	···	1.90	1.98

of bound-state potentials on light-ion data. The results are given in Table VII and are quite similar to those obtained for the ^{208}Pb(^{16}O, ^{15}N) reaction; in making a comparison allowance must be made for the fact that finite-range and nonlocality effects were included in the (^{3}He, d) reanalysis of Ref. 9, but were not used in Ref. 29. As can be seen in Table VII, the relative strengths predicted with the two bound-state potentials are quite similar despite the fact that the absolute strengths differ by approximately a factor of 2. Moreover, the changes are independent of the bombarding energy to an accuracy of 5 to 8% over the range 100 to 200 MeV. The position and shape of the angular distributions are found to be influenced only slightly by the change in the bound-state potential.

It is well known that the normalization of the transfer amplitude is proportional to the asymptotic normalization of the bound-state wave functions, so that if ϕ is the bound-state wave function, and S is the spectroscopic factor $\sqrt{S}\,\phi(r)$ for large r is the quantity that is determined by normalization of a DWBA to a measured cross section. This quantity is $(2Mr/\hbar^2)^{1/2}$ times the reduced-width amplitude $\gamma(r)$ that appears in treatments[30] of nucleon-nucleus resonance reactions.

In Table VII we also show the ratios of the ^{209}Bi bound-state wave functions for the two potentials considered. As can be seen, the square of the ratio of the asymptotic values of the wave functions is within 5% of the ratios of the corresponding transfer cross sections. The two ratios are even closer if one uses the ratio of the wave functions evaluated at r=10 fm. For r< 8 fm, the two bound-state wave functions are quite different and their ratio varies rapidly with r. These results confirm that the DWBA amplitudes are sensitive only to values of the target bound-state wave function for r> 9 fm.

2. ^{207}Pb bound-state wave functions

The proper choice of the potential for the ^{207}Pb neutron-hole system is less clear than for ^{209}Bi. Several attempts[27, 31, 32] have been made to fit the single-neutron-hole level structure of ^{207}Pb and all have resulted in potentials with surprisingly large radii (an example is potential Pb2 in Table X; it has r_r =1.36 fm). Such potentials give an rms radius[27] for the neutron distribution in ^{208}Pb that is about 0.42 fm larger than currently accepted values.[33-35] In addition, when used in the analysis of light-ion reactions, the potentials fitted to the ^{207}Pb levels give DWBA cross sections some two to three times too large if reasonable spectroscopic factors (around unity) are assumed.[27, 28, 36] We have therefore used a ^{207}Pb potential[9, 28] with a more conventional geometry. This potential accurately reproduces the measured[37, 38] neutron-hole radii in ^{207}Pb (a very recent reanalysis[39] of the rms neutron radius in ^{208}Pb disagrees slightly with these numbers) and has parameters close to those obtained by extrapolation to zero bombarding energy of the optical potentials[40, 41] found for neutron scattering from ^{208}Pb. The light-ion transfer predictions obtained with this potential are also quite reasonable.[28] The well depth varies by ±2.5% in fitting the six single-hole states in ^{207}Pb, a larger state-to-state variation than that encountered in the ^{209}Bi system.

DWBA predictions using potentials Pb1 and Pb2 (the latter is a large-radius potential that was fitted[27] to the ^{207}Pb levels) have been compared. Potential Pb2 gives DWBA cross sections some 2 to 2.5 times larger than potential Pb1. The ratios are again nearly independent of the bombarding energy and are also roughly the same for transitions leaving ^{17}O in its $1d_{5/2}$ and $2s_{1/2}$ single-particle states. We have also compared cross sections obtained using potentials Pb1 and Pb3, both of which were also used to analyze[28, 42] ^{208}Pb(d, t)^{207}Pb and ^{208}Pb(^{3}He, α)^{207}Pb data. The ratios of cross sections with Pb1 and Pb3 for the (d, t), (^{3}He, α), and (^{16}O, ^{17}O) reactions are the same to within a few percent. The shapes of the (^{16}O, ^{17}O) angular distributions predicted using these three bound-state potentials are almost identical.

It is found that, as in the case of single-proton transfer, the effect of changes in bound-state parameters on absolute DWBA cross sections for the neutron-transfer reactions (^{16}O, ^{17}O) (d, t), and (^{3}He, α) is given to within 5% by the ratios of the asymptotic bound-state wave functions.

3. ^{15}N and ^{17}O bound-state wave functions

The light-ion potential of Ref. 10 was used for both the ^{15}N and ^{17}O vertices. This potential results in an rms charge radius for ^{16}O of 2.636 fm which is slightly smaller than the average value of 2.707 ± 0.015 found in three recent electron-scattering studies.[43-45] When used for ^{17}O it gives a slightly large charge radius (2.703 compared to[43] 2.662 ± 0.026). Calculations with other parameters for ^{15}N and ^{17}O showed that significantly smaller changes in the absolute cross sections are obtained than those that result from similar variations of ^{207}Pb and ^{209}Bi bound-state parameters. These changes are again nearly independent of bombarding energy and are closely related to the asymptotic values of the projectile bound-state wave functions. The shapes of the predicted angular distributions are insensitive to the bound-state parameters.

D. Accuracy of DWBA calculations

Finite-range DWBA computations have become commonplace during the past few years; however, it should be noted that due to the high bombarding energies, massive target, and large bound-state angular momenta involved in this study, the calculations reported here are far from routine, given the present state of the art. The calculations for the higher excited states (which are weakly bound and hence have slowly decaying wave functions) require form-factor integrals that extend to 40 fm and thus encompass some 85 wavelengths at 216.6 MeV. Partial waves up to $l = 240$ were included in the 216.6-MeV calculations. Five angular momentum transfers are involved in most of the [^{16}O, ^{17}O(g.s.)] reactions. In all cases, integration parameters and angular momentum ranges were chosen such that the peak differential cross sections are computed to an accuracy of 0.5%.

E. Summary

This section contains a complete specification of the wave functions and the effective interaction used in the DWBA calculations for the reactions ^{208}Pb(^{16}O, ^{15}N)^{209}Bi and ^{208}Pb(^{16}O, ^{17}O)^{207}Pb and a discussion of the sensitivity of the calculated cross sections to variations in the parameters of bound-state and scattering potentials. The main conclusions of the discussion of sensitivity to parameter variations are as follows:

(1) Optical potentials that yield high-quality fits to elastic scattering yield DWBA cross sections that agree to within a few percent in the vicinity of the grazing-angle peak.

(2) Reasonable variations in the bound-state parameters can change absolute DWBA cross sections at a given bombarding energy by as much as a factor of 2. These changes are, however, almost independent of bombarding energy and are weakly state dependent.

(3) The ratio of the absolute DWBA cross sections computed with two different bound-state wave functions is given to within 5 or 10% by the ratio of the asymptotic bound-state wave functions.

V. COMPARISON OF EXPERIMENT AND DWBA

A. ^{208}Pb(^{16}O, ^{15}N) ^{209}Bi angular distributions

The solid curves in Fig. 4 are the DWBA predictions for the ^{208}Pb(^{16}O, ^{15}N)^{209}Bi transfer reactions using optical potential *I*3 (Table IV), bound-state potentials O1 and Bi1 (Table VI), and the spectroscopic factors (labeled "present study") given in Table VIII. The extraction of the spectroscopic factors is discussed later in this section. The dashed curves are the same DWBA predictions shifted in angle and renormalized to fit the data. The required angle shifts are given in Table IX. Similar results are obtained with the other optical potentials given in Sec. III.

The reaction ^{208}Pb(^{16}O, ^{15}N)^{209}Bi has previously been measured at a bombarding energy of 69.1 MeV by Barnett *et al.*[4] Data were reported for transitions to the $2f_{7/2}$, $1i_{13/2}$, and the superimposed $2f_{5/2}$ and $3p_{3/2}$ states of ^{209}Bi with ^{15}N left in its

TABLE VIII. Spectroscopic factors for proton stripping reactions to single-proton levels in ^{209}Bi. The table contains relative spectroscopic factors; the asterisks indicate the value that was used to normalize each set of spectroscopic values. The resulting N_j [see Eq. (5.1)] are given in the last row of the table.

Reaction:	(^{16}O,^{15}N)	(^{12}C, ^{11}B)	(^{11}B, ^{10}Be)	(^{3}He,*d*)	(^{3}He,*d*)	(^{3}He,*d*)	Theory
E_{lab} (MeV):	104, 138.5, 216.6	97.9	72.2	20.3	44.2	51.3	···
Ref.:	Present study	11	9[b]	60	62	9	57
nl_j							
$1h_{9/2}$	0.95*	0.76	0.74	1.10	0.59	0.61	0.83
$2f_{7/2}$	0.74	0.74*	0.74*	0.74*	0.74*	0.74*	0.74*
$1i_{13/2}$	0.61	0.68	0.88	0.53	0.55	0.59	0.61
$2f_{5/2}$	0.61	0.49	0.51	0.83	0.72	0.69	0.58
$3p_{3/2}$	0.55	0.63	0.82	0.63	0.64	0.66	0.64
$3p_{1/2}$	0.52	···	···	0.46	0.39	···	0.47
N_j:	2.26, 1.29, 0.75[a]	1.10	0.97[c]	1.06	1.61	0.88	1.15

[a]Based on optical potential *I*3.

[b]Average of values for optical potentials 1 and 2.

[c]Based on our reanalysis using core-Coulomb corrections to the DWBA effective interaction.

TABLE IX. Angle shifts required to match the DWBA calculations for the ^{208}Pb(^{16}O, ^{15}N)^{209}Bi reaction to the data. Optical potential *I*3 was used. A negative value indicates that the DWBA distribution peaked at too large an angle.

State	Shift (deg)		
	104 MeV	138.5 MeV	216.6 MeV
$1h_{9/2}$	−0.5 ± 0.4	−1.4 ± 0.2	−2.2 ± 0.2
$2f_{7/2}$	−1.9 ± 0.3	−1.5 ± 0.1	−1.6 ± 0.1
$1i_{13/2}$	−3.6 ± 0.3	−2.1 ± 0.1	−2.6 ± 0.2
$2f_{5/2}$	−2.7 ± 0.3	−1.7 ± 0.2	−1.2 ± 0.1
$3p_{3/2}$	−3.1 ± 0.3	−1.4 ± 0.2	−1.9 ± 0.2
$3p_{1/2}$	−2.9 ± 0.6	−1.6 ± 0.3	−1.7 ± 0.3

ground state. Figure 12 shows these data and the results of DWBA calculations for the appropriate transitions; the curves have the same significance as in Fig. 4 except that no angle shift was used in deriving the dashed curves. The DWBA calculations were made with the optical potential *Q* as evaluated at 104 MeV. The precise values of the nuclear optical-model parameters are in fact almost irrelevant at these sub-Coulomb energies; indeed pure Coulomb-distorted waves yield cross sections that are the same to within 0.5%.

The main conclusions to be drawn from Figs. 4 and 12 and Table IX are as follows:

(1) The shapes of the angular distributions are reasonably reproduced by the DWBA at all bombarding energies.

(2) The DWBA distributions peak at systematically larger angles than the data. At 104 MeV this shift increases from only −0.5° for the ground state to −3° for the $3p_{1/2}$ state and has already been discussed in the literature.[6,13] At 138.5 MeV the shift is −1.4° for the ground state and increases slowly with excitation energy, while at 216.6 MeV the shift, although still substantial (~2° or 10% of the peak angle), is almost independent of excitation energy.

(3) The renormalization factors required to bring the peak DWBA and measured cross sections into agreement vary significantly with energy but in a nearly state-independent manner; DWBA cross sections are too small by a factor of about 2 at 104 MeV and too large by 25% at 216.6 MeV. This failure of the DWBA to correctly predict the energy dependence of the absolute cross sections is discussed in detail in a later section.

B. ^{208}Pb(^{16}O, ^{17}O) ^{207}Pb angular distributions

The analysis of the ^{208}Pb(^{16}O, ^{17}O)^{207}Pb data is complicated by the fact that, except for groups 1 and 2, each of the observed peaks consists of

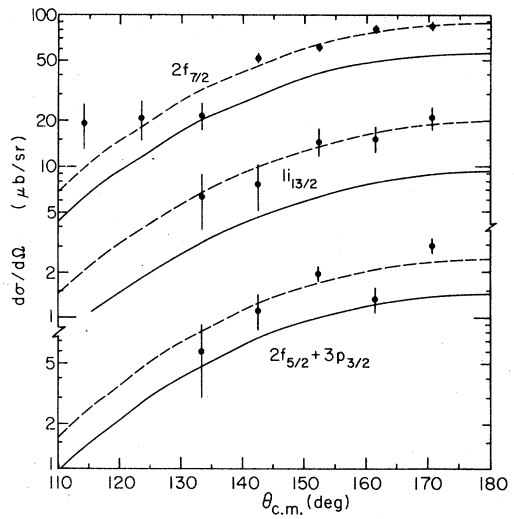

FIG. 12. Differential cross sections for the ^{208}Pb(^{16}O, ^{15}N)^{209}Bi reaction at 69.1 MeV. The solid lines are DWBA calculations using optical potential *Q* evaluated at 104-MeV, bound-state potentials O1 and Bi1 and the spectroscopic factors of Table VIII. The dashed curves are these calculations renormalized to best fit the data. The data are from Ref. 4.

unresolved transitions to different states in ^{207}Pb with ^{17}O left either in its $1d_{5/2}$ ground state or $2s_{1/2}$ excited state. Thus the ratio of the spectroscopic factors for these two states in ^{17}O influences the analysis of the data. As will be discussed later, we found that a ratio of 0.74 seems to be preferred in our analysis. Figure 7 shows the resulting DWBA predictions for the six ^{17}O groups observed in the spectra. The solid curves are the DWBA calculations using optical potential *I*3 (Table IV), bound-state potentials O1 and Pb1 (Table VI), and the spectroscopic factors (labeled "present study") of Table X. For groups 3–6 the appropriate transitions given in Table I were summed. The dashed lines are the results of shifting and renormalizing the DWBA predictions to fit the data; the resulting angle shifts are given in Table XI. DWBA predictions obtained with the other potentials given in Sec. III are very similar to those shown in Fig. 7. The main conclusions to be drawn from Fig. 7 and Table XI are as follows:

(1) With the exception of the $1h_{9/2}$ state the DWBA again successfully predicts the shape of the angular distributions. The minima in the distributions at angles forward of the peak provide a more stringent test than is available in the (^{16}O, ^{15}N) reaction; the data are consistent with the minima although further measurements at intermediate angles are necessary to establish more firmly the existence of the minima in the measured cross sections. The calculated minima are

TABLE X. Spectroscopic factors for neutron pickup reactions to ^{207}Pb. The table contains relative spectroscopic factors that were normalized to $S^{Pb}_{1/2} = 1.9$. The resulting N_j [see Eq. (5.2)] are given in the last row of the table. The spectroscopic factors have also been divided by $2j+1$.

Reaction:	(^{16}O, ^{17}O)	(^{12}C, ^{13}C)	(^{11}B, ^{12}B)	(p,d)	(p,d)	(p,d)	(d,t)	(d,t)	(^{3}He, α)	Theory
E_{lab} (MeV):	104, 138.5, 216.6	97.9	72.2	22	35	40	8–11.5	50	47.5	···
Ref:	Present study	11	9	61	64	63	9	9	42	51
nl_j										
$3p_{1/2}$	0.95	0.95	0.95	0.95	0.95	0.95	0.95	0.95	0.95	0.95
$2f_{5/2}$	0.80	0.83	0.87	0.77	0.92	0.92	0.87	0.83	0.76	0.94
$3p_{3/2}$	1.07	0.84	1.27	0.90	0.84	0.88	1.27	0.84	0.98	0.92
$1i_{13/2}$	0.34	0.69	···	···	0.54	0.92	···	0.69	0.59	0.87
$2f_{7/2}$	0.80	0.64	0.68	0.68	0.56	0.69	0.68	0.64	0.80	0.70
$1h_{9/2}$	0.75	···	···	···	0.60	0.65	···	···	0.36	0.84
N_j:	1.16, 0.81, 0.61[a]	1.04	1.32	1.09	0.95	1.08	1.32	1.04	1.63	1

[a]Based on optical potential *I*3.

discussed in the following subsection.

(2) The angle shifts given in Table XI at 104 MeV show some tendency to increase with increasing excitation energy, as was the case for the (^{16}O, ^{15}N) reaction; at the higher bombarding energies the shifts are negligible.

(3) As is the case for the (^{16}O, ^{15}N) reaction, the absolute DWBA cross sections increase more rapidly with bombarding energy than the measured cross sections. The discrepancy is, however, significantly less than for the (^{16}O, ^{15}N) reaction and, in fact, agreement with experiment is quite good at 104 and 138.5 MeV.

C. Minima in the ^{208}Pb(^{16}O, ^{17}O)^{207}Pb cross sections

As was mentioned above, the calculated angular distributions for the reaction ^{208}Pb(^{16}O, ^{17}O)^{207}Pb show deep minima. The dip predicted at 34° in the 138.5-MeV DWBA cross section is particularly interesting; it is one to two orders of magnitude deep and appears in the angular distributions for transitions to all the states in both ^{207}Pb and ^{17}O. (For the $1h_{9/2}$ state in ^{207}Pb it is filled in to a significant extent.) The minimum persists when the optical potential is changed; it is also insensitive to changes in the bound-state wave functions. Weaker minima occur in the (^{16}O, ^{17}O) cross sections at 104 at 216.6 MeV.

TABLE XI. Angle shifts required to match the DWBA calculations for the ^{208}Pb(^{16}O, ^{17}O)^{207}Pb reaction to the data. Optical potential *I*3 was used with the spectroscopic factors of TABLE X.

Group	Shift (deg)		
	104 MeV	138.5 MeV	216.6 MeV
1	−0.1 ± 0.2	0.0 ± 0.1	0.6 ± 0.3[a]
2	0.1 ± 0.2	0.3 ± 0.1	−0.6 ± 0.4
3	−0.2 ± 0.2	0.1 ± 0.1	−1.0 ± 0.3
4	−1.8 ± 0.2	−0.4 ± 0.1	−0.2 ± 0.3
4a	−2.2 ± 0.4		
4b	−1 ± 0.4		
5		0.0 ± 0.2	−0.6 ± 0.2
6	0 ± 0.4[a]	0.1 ± 0.3[a]	−0.2 ± 0.5[a]

[a]Shifted DWBA is not a good fit to the data.

Fuller and Moffa[46] have shown, and we have confirmed for the present case, that minima of this kind stem from the interference of the transfer amplitudes arising from two different classical orbits leading to the same deflection angle. The contributing orbits here are the outermost, purely repulsive, Coulomb orbit and a still peripheral orbit in which a small nuclear attraction partially cancels a stronger Coulomb repulsion. Following Fuller and Moffa we refer to these as the "outer" and "inner" trajectories.

The occurrence of the deep minimum requires that the two amplitudes be of nearly equal magnitude. The magnitude of the inner contribution is sensitive to the absorptive part of the optical potential at separations down to the distance of closest approach. It has been established[3] that this absorption is well determined by the elastic data and hence should be nearly the same for all the optical potentials we use. The outer orbit is, of course, a pure Coulomb orbit; the magnitude of its contribution is determined by the degree of mismatch of the Coulomb wave functions for large orbital angular momentum and by the tail of the target wave function. Both of these determining factors are independent of the optical potential.

Also the decay rate of the ^{207}Pb wave function changes by only 10% between the $3p_{1/2}$ and $2f_{7/2}$ states. Thus it is reasonable that the minimum appears in transitions to all of the first five states in ^{207}Pb and for all the optical potentials considered here.

D. Extraction of relative spectroscopic factors

Figures 4 and 7 show that it is not reasonable in this analysis to extract spectroscopic factors by the usual procedure of dividing observed cross sections by DWBA estimates, since such ratios would vary significantly with bombarding energy. It is, however, possible to devise a modified analysis wherein the DWBA cross sections are multiplied by *ad hoc* energy-dependent normalization factors and to determine relative spectroscopic factors from the total (angle-integrated) transfer cross sections given in Tables II and III. For the (^{16}O, ^{15}N) reactions, the renormalized DWBA total cross section is given by

$$\sigma_{\mathrm{Th}}(j,E_i)=N(E_i)S^p S_j^{\mathrm{Bi}}\sigma(j,E_i) \tag{5.1}$$

where E_i is the bombarding energy and j labels a single-particle state in ^{209}Bi. S^p is the spectroscopic factor at the projectile vertex ($^{16}\mathrm{O}\rightarrow{}^{15}\mathrm{N}+p$). We use the full single-hole value $S^p=2$; a shell-model calculation[47] indicates $S^p=1.66$ while analyses of light-ion pickup experiments[48-50] yield values scattered over the range $1.3<S^p<2.8$. S_j^{Bi} is the spectroscopic factor for the single-particle state j of ^{209}Bi; $N(E_i)$ is an energy-dependent renormalization factor and $\sigma(j,E_i)$ is the DWBA total cross section with unit spectroscopic factors at both vertices. The normalization factors $N(E_i)$ and the spectroscopic factors S_j^{Bi} are determined by a least-squares fit to the observed total cross sections (Table II). Only the relative values of S_j^{Bi} obtained from this analysis are significant; the absolute values depend on the overall normalization chosen for the factors $N(E_i)$. We use the value $S_{9/2}^{\mathrm{Bi}}=0.95$ for the ^{209}Bi ground state, as obtained by Ring and Werner[51] in a vibration-particle coupling calculation. There are then eight parameters [$3N(E_i)$ and $5\,S_j^{\mathrm{Bi}}$] to be determined by fitting 18 measured total cross sections. The relative spectroscopic factors obtained are given in Table VIII.

For the (^{16}O, ^{17}O) reactions we must consider both ground and first-excited states of ^{17}O. We then fix the ground-state spectroscopic factors at $S_{5/2}^p=1$ at the projectile and $S_{1/2}^{\mathrm{Pb}}=1.9$ at the target vertex.[51] Shell-model calculations[47] indicate $S_{5/2}^p\simeq 0.93$ for the ^{17}O ground state, while analyses of light-ion stripping experiments[52-55] yield values in the range $0.8<S_{5/2}^p<1$. There are then nine parameters [$3N(E_i)$, $S_{1/2}^p$, and $5\,S_j^{\mathrm{Pb}}$] to be determined from the 18 independent measured cross sections given in Table III. The resulting relative spectroscopic factors are given in Table X. The value $S_{1/2}^p=0.74$ is lower than would be expected from a detailed shell-model calculation[47] which gives $S_{1/2}^p/S_{5/2}^p=1.02$ or from light-ion experiments[52-55] which, although somewhat ambiguous, are generally consistent with $S_{1/2}^p\sim S_{5/2}^p$. However, the smaller value of $S_{1/2}^p$ is strongly indicated by the present analysis; increasing $S_{1/2}^p$ to 1 raises the χ^2 by a factor of more than 2 and reduces the already small value of $S_{13/2}^{\mathrm{Pb}}$ to absurdly small or even negative values. If $S_{13/2}^{\mathrm{Pb}}$ is constrained to a "reasonable" value, such as 12, χ^2 for $S_{1/2}^p=1$ is very high and the minimum χ^2 occurs for $S_{1/2}^p=0.55$.

The success of the DWBA in predicting the relative spectra of the transfer reactions is shown in Figs. 13 and 14 which compare experimental spectra at a fixed scattering angle near the peak with values computed using the spectroscopic factors of Tables VIII and X. The theoretical cross sections have been normalized by the energy-dependent normalization factors $N(E_i)$ given in the figures. The overall χ^2 per point for the spectra shown are 2.2 for the (^{16}O, ^{15}N) reaction and 1.9 for the (^{16}O, ^{17}O) reaction. These correspond to rms relative errors of 11% and 15%, respectively. [The biggest sources of error for the (^{16}O, ^{17}O) reaction are the poorly reproduced $1h_{9/2}$ states. If they are ignored, one obtains a χ^2 per point of 0.8 and an rms relative error of 9%.]

Figure 13 also shows the predicted spectrum for transitions in which ^{15}N is left in its 6.32-MeV $1p_{3/2}^{-1}$ excited state. As can be seen, transitions to this state are predicted to be important at the higher bombarding energies. Because the ^{15}N decays in flight, the peaks corresponding to these transitions will be Doppler-broadened by about 1 MeV. Thus, the transitions to the various states in ^{209}Bi are unresolved. In Fig. 2 strong yields in the region of 6- to 10-MeV excitation energy are observed in the 138.5-MeV and 216.6-MeV spectra. If we assume that the $^{15}N^*$ decays isotropically, we can predict a theoretical Doppler-broadened spectrum. Such spectra are presented as shaded histograms in Fig. 2. The energy-dependent normalization factors of Fig. 13 have again been applied. We see that the production of ^{15}N in its 6.32-MeV state accounts for approximately one-half of the strength observed in the 6- to 10-MeV excitation range. Thus from Figs. 13, 14, and 3, we see that DWBA does remarkably well in predicting the dependence on bombarding energy of the relative cross sections of transitions to different states in the target and projectile.

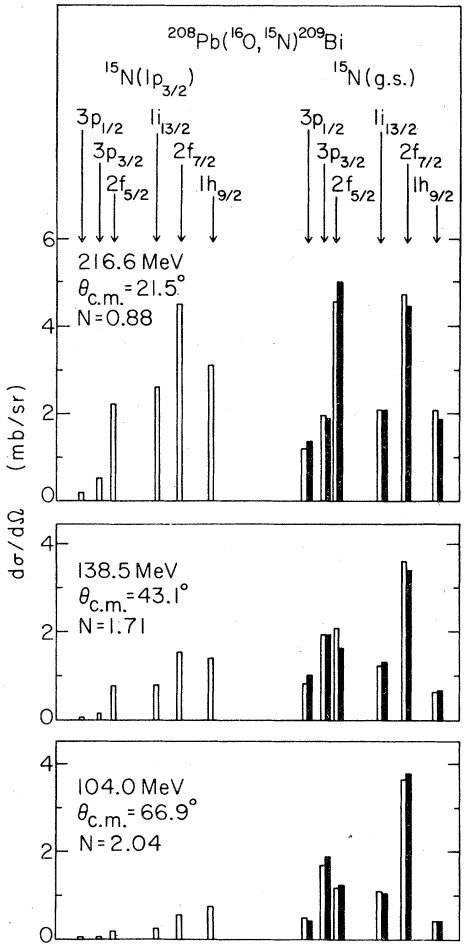

FIG. 13. Comparison of experimental and DWBA spectra for the ^{208}Pb(^{16}O, ^{15}N)^{209}Bi reaction. The solid bars give the experimental differential cross sections for the indicated transitions. The open bars represent the DWBA calculations made with optical potential *Q*, bound-state potentials O1 and Bi1 and the spectroscopic factors of Table VIII. The calculations have been renormalized by the normalizations (*N*) given in the figure.

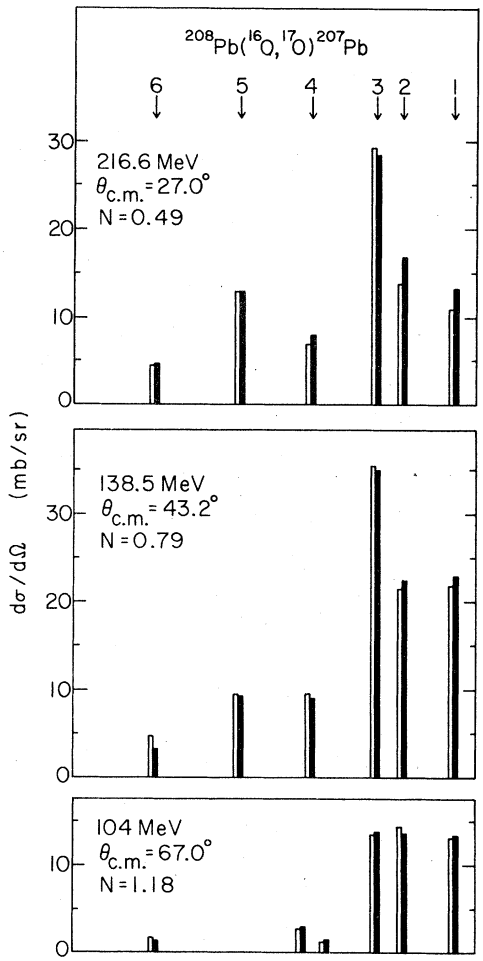

FIG. 14. Comparison of experimental and DWBA spectra for the ^{208}Pb(^{16}O, ^{17}O)^{207}Pb reaction. The caption of Fig. 13 applies except that the bound-state potentials O1 and Pb1 and the spectroscopic factors of Table X were used.

VI. ENERGY DEPENDENCE OF TRANSFER CROSS SECTIONS

In Sec. V it was shown that finite-range DWBA calculations predict angular distributions whose shapes agree fairly well with those observed for the (^{16}O, ^{15}N) and (^{16}O, ^{17}O) reactions on ^{208}Pb. DWBA is also remarkably successful in accounting for the relative intensities of transitions to different single-particle and single-hole states at the three bombarding energies studied. The ratios of DWBA and experimental cross sections are, however, strikingly energy dependent.

Consider first the transfer cross sections integrated over angles and summed over individual final states. These summed single-particle transfer cross sections are shown as functions of bombarding energy in Fig. 15. For (^{16}O, ^{15}N) reactions, transitions to single-particle states up to and including the $3p_{1/2}$ level at 3.64 MeV in ^{209}Bi were included, with ^{15}N in its ground state; for (^{16}O, ^{17}O) single-hole states up to and including the $1h_{9/2}^{-1}$ level at 3.47 MeV in ^{207}Pb were included, with ^{17}O in its ground or first-excited $2s_{1/2}$ state. The lines give the DWBA predictions with the four representative optical potentials discussed in Sec. III; experimental cross sections are indicated by dots. The same qualitative behavior is found for (^{16}O, ^{15}N) and (^{16}O, ^{17}O) reactions: After a rapid increase through the Coulomb barrier, the experimental summed cross sections level off at around 100 MeV, and start to decrease steadily with bom-

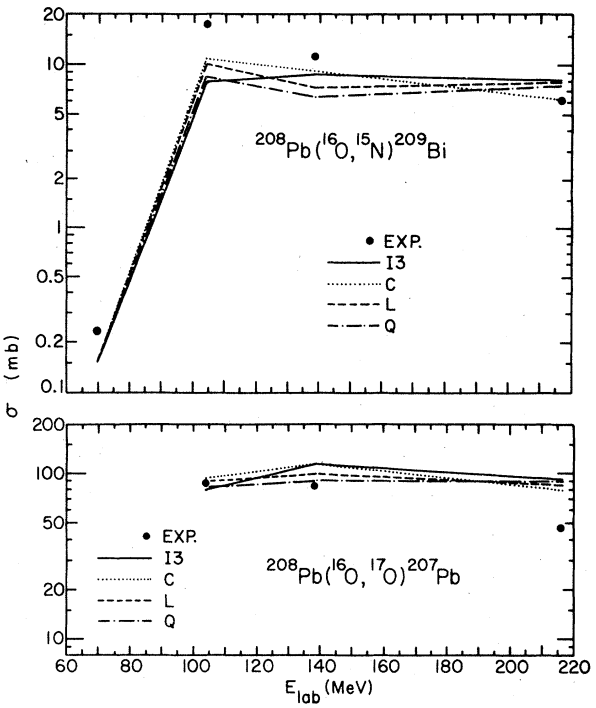

FIG. 15. Total ^{208}Pb(^{16}O, ^{15}N)^{209}Bi (top) and ^{208}Pb(^{16}O, ^{17}O)^{207}Pb (bottom) cross sections. The top section shows the angle-integrated cross sections for producing ^{15}N in its ground state and ^{209}Bi in any of its single-proton states. The bottom section shows the angle-integrated cross sections for ^{17}O in either its ground state or $2s_{1/2}$ (0.87 MeV) excited state and ^{207}Pb in any of its neutron-hole states. The dots are the experimental total cross sections; the errors are about the size of the dots. The curves are the results of DWBA calculations made with the indicated optical potentials, bound-state potentials O1 and Bi1 or Pb1 and the spectroscopic factors in Tables VIII and X.

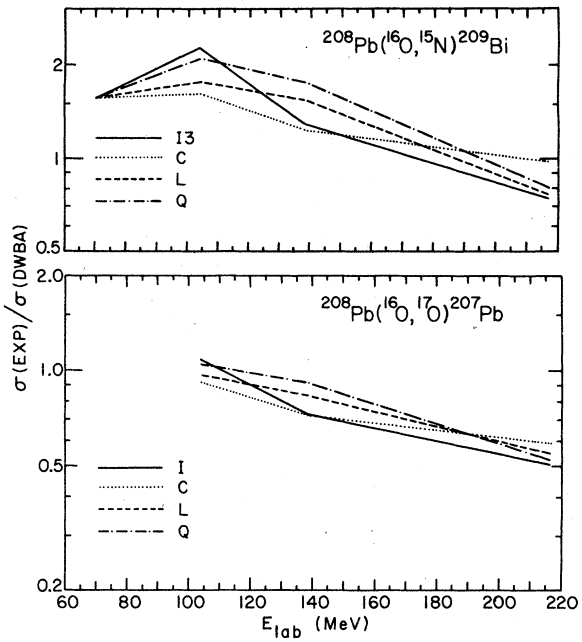

FIG. 16. Ratios of the ^{208}Pb(^{16}O, ^{15}N)^{209}Bi (top) and the ^{208}Pb(^{16}O, ^{17}O)^{207}Pb (bottom) cross sections. Shown are the ratios σ (exp)/σ (DWBA) of the cross sections given in Fig. 15.

barding energy. The DWBA cross sections, after reproducing the observed increase of nearly two orders of magnitude through the Coulomb barrier, level off and remain almost constant with increasing energy. At 216.6 MeV, the DWBA cross sections are clearly too large.

The relation between theoretical and experimental energy dependence is exhibited more clearly in Fig. 16. Here the ratio σ(exp)/σ(DWBA) is plotted as a function of bombarding energy for the summed cross sections shown in Fig. 15. If the DWBA predictions for the energy dependence were correct, these curves would be horizontal straight lines. Instead, the curves representing σ(exp)/σ(DWBA) fall off with increasing energy, with the slope greater for (^{16}O, ^{15}N). The ratio of experimental to DWBA cross sections varies by a factor of 3 between 104 and 216.6 MeV for (^{16}O, ^{15}N), and by a factor of 2 for (^{16}O, ^{17}O). It is clear that DWBA predicts an incorrect energy dependence.

These conclusions are confirmed and reinforced in the accompanying paper[56] which reports measurements of the stripping reactions (^{16}O, ^{15}N) and (^{16}O, ^{15}O) on ^{208}Pb at 312.6 MeV. The ratio σ(exp)/σ(DWBA) for (^{16}O, ^{15}N) decreases by an additional factor of 2 between 216.6 and 312.6 MeV—roughly what would be indicated by extrapolation of the curves in Fig. 16. The (^{16}O, ^{15}O) cross-section ratio is found to decrease between 139 and 312.6 MeV by about the same amount as the (^{16}O, ^{15}N) cross section. Results are thus available for three single-nucleon transfer reactions on ^{208}Pb; one [(^{16}O, ^{17}O)] is quite well matched, one [(^{16}O, ^{15}O)] is badly mismatched, and the third [(^{16}O, ^{15}N)] is moderately mismatched. All exhibit cross sections that, when summed over a fixed number of channels, start just above the Coulomb barrier to decrease steadily with bombarding energy; the DWBA cross sections, for a wide variety of optical potentials (all fitting the elastic cross sections to at least a moderate extent) and bound-state form factors (cf. Table XI), decrease much too slowly or remain constant with energy.

It was emphasized in Sec. V that DWBA correctly reproduces at each energy the relative intensities of transitions to different single-particle and single-hole states. This implies that the dis-

crepancy in the energy dependence noted above is essentially state independent. Figure 17 confirms the state independence of the ratio $\sigma(\text{exp})/\sigma(\text{DWBA})$ for optical-model fit *I*3 (independent fit at each energy); indeed the differences between the curves for different final states in ^{209}Bi and ^{207}Pb are distinctly smaller than the differences between curves for different optical potentials.

We believe that this discrepancy between DWBA and experiment is significant. It cannot be removed by reasonable parameter variations within the limits of conventional DWBA analyses. Note in particular that although uncertainties in the bound-state form factors make the calculated absolute cross sections at each energy uncertain by ± 50% or more, form-factor modifications tend to influence the cross sections at all energies in the same way. Thus the slopes of the curves $\sigma(\text{exp})/\sigma(\text{DWBA})$ given in Figs. 16 and 17 are much less sensitive to the bound-state form factors than are the absolute normalizations.

Three possible ways of accounting for the discrepancy come to mind. One involves energy-dependent modification of the bound-state form factors. Pruess *et al.*[57] have suggested that the heavy-ion cores in a reaction such as (^{16}O, ^{15}N) strongly polarize the orbit of the transferred valence nucleon. This effect permits transfer to occur at much larger core-core separations than is possible without polarization. Estimates of the polarization effect suggest that it considerably increases the transfer cross sections close to the Coulomb barrier and that its influence diminishes with increasing energy; such an effect would tend to reduce the discrepancy between theory and experiment observed here. However, the polarization effect would be expected to be significantly state dependent, and it is somewhat difficult to imagine it producing a factor of 2 between 216.6 and 312.6 MeV.

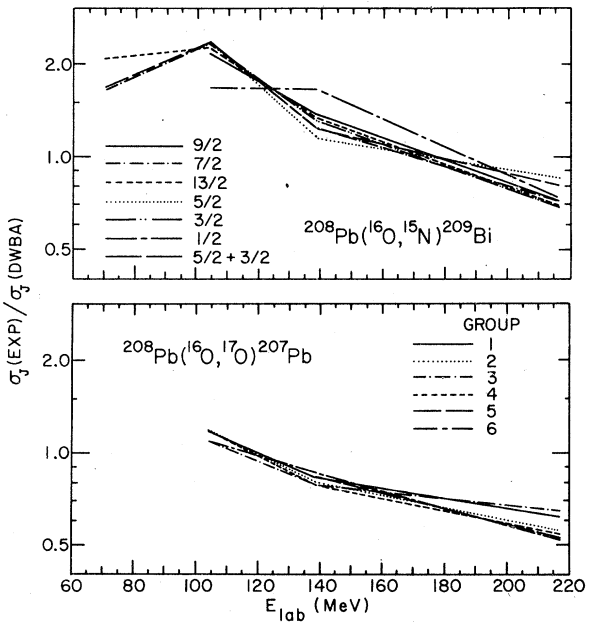

FIG. 17. Ratios of the ^{208}Pb(^{16}O, ^{15}N)^{209}Bi cross sections for each single-proton state in ^{209}Bi (top) and of the ^{208}Pb(^{16}O, ^{17}O)^{207}Pb cross sections for each group identified in Table I (bottom). Shown are σ_j (exp)/σ_j (DWBA) where the DWBA calculations were made with the assumptions of Fig. 15 (optical potential *I*3 was used).

A second possibility is to replace the single-channel optical-model wave functions by multi-channel states in which low-lying collective excitations of the various nuclei involved are explicitly included. Unless the major effects of the coupling to inelastic channels are on the elastic-channel wave functions, it is hard to see how few-channel calculations of this sort could yield state-independent corrections to DWBA.

A third possibility is to remain within the optical-model-DWBA framework but to remove the severe restrictions (local Woods-Saxon form, *L* independence) so far placed on the optical potential. It seems unlikely that this approach will completely remove the energy discrepancy (without abandoning detailed elastic fits) in view of the severe constraints that fitting the elastic data with conventional potentials has been found to place on the distorted waves. On the other hand, in collisions in which at least one of the nuclei involved has mass less than 40, a transition occurs at bombarding energies of 1.5 to 2 times the Coulomb barrier from a low-energy region in which fusion accounts for most of the reaction cross section to a high-energy region in which strongly damped processes predominate.[58] Although there are no data for the system ^{16}O + ^{208}Pb in the transition region (130 to 180 MeV), measurements for this system near the Coulomb barrier[1] and at 312.6 MeV[59] indicate that at some intermediate energy flux starts to pour out of complete fusion into strongly damped processes. Such processes are believed to be direct, to involve large energy transfer, and to be localized in angular momentum in roughly the same way as the peripheral reactions under consideration here. Strong coupling to such processes might involve so many channels that an optical-model treatment of the peripheral channels remains possible; however, their strong localization in *L* makes it unlikely that the local, *L*-independent potential forms familiar from light-ion physics will be appropriate. The very fact that the energy discrepancy between DWBA and experiment is so strikingly state independent suggests

that an interpretation within the optical-model-DWBA framework is worth seeking.

VII. COMPARISON WITH EARLIER STUDIES

Many studies have been reported in which spectroscopic factors were extracted for the single-nucleon transfer reactions on ^{208}Pb. There is also some evidence on the energy dependence of single-nucleon transfer reactions induced by heavy ions on ^{208}Pb and on the extent to which DWBA calculations reproduce this energy dependence. We show in this section that our results are in general agreement with those of earlier studies.

Previous single-proton stripping and single-neutron pickup studies on ^{208}Pb include heavy-ion experiments,[4,9,11,12] with ^{11}B, ^{12}C, and ^{16}O beams and a variety of light-ion induced reactions.[9,42,60-64] In these papers the approach customary in light-ion studies has been used: The spectroscopic factor at the light-ion vertex is regarded as known, and normalization of the DWBA cross section to the observed absolute cross section determines a spectroscopic factor for a single-particle or single-hole state. Such analyses fix the ratios of the spectroscopic factors of different states with a fairly high degree of reliability but have uncertainties in the absolute normalization that are sizable and very difficult to assess. We therefore start by comparing relative spectroscopic factors and return to a discussion of the absolute normalizations later.

Tables VIII and X summarize the relative spectroscopic factors and absolute normalizations derived in this and previous studies of proton stripping and neutron pickup reactions on ^{208}Pb. To facilitate comparison with our spectroscopic factors, the spectroscopic factors of the previous studies have been renormalized. For the neutron pickup analyses summarized in Table X the spectroscopic factors are normalized to $S^{\mathrm{Pb}}_{1/2}/(2j+1) = 0.95$ and the additional normalization factors given in the last row of the table. The procedure was modified slightly in presenting the proton-stripping results in Table VIII. The $h_{9/2}$ ground-state transition is relatively weak in all the reactions considered here, and a considerably smaller scatter in relative spectroscopic factors results if we normalize to $S^{\mathrm{Bi}}_{7/2} = 0.74$, the spectroscopic factor of the much more strongly excited $2f_{7/2}$ state.

As is clear from Tables VIII and X the relative spectroscopic factors, including the ones derived in the present study, are remarkably consistent. They are also in good agreement with the calculated spectroscopic factors of Ring and Werner.[51] The one notable exception is the anomalously low value $S^{\mathrm{Pb}}_{13/2} = 0.34$ found here for the (^{16}O, ^{17}O) reactions. However, the strongest transition to the $1i_{13/2}$ state is only a small part of group 4, and, as was discussed in Sec. V, the spectroscopic factor quoted for the $1i_{13/2}$ state is quite uncertain.

Single-proton stripping and single-neutron pickup reactions have been studied at the Oak Ridge cyclotron laboratory.[9,11,12] The more recent ^{12}C study[11] measured transfer cross sections at a bombarding energy of 97.9 MeV. Since the authors express reservations about the accuracy of the absolute cross sections measured in the previous experiments[12] at 77.4 and 116.4 MeV, we conclude that nothing significant can be said at present about the energy dependence of the ^{12}C-induced transfer cross sections and concentrate on the 97.9-MeV data. The value of E/E_B for ^{12}C + ^{208}Pb at 97.9 MeV is 1.6, quite close to the value of 1.7 for our 138.5-MeV data. We therefore compare the 97.9-MeV ^{12}C data with the 138.5-MeV ^{16}O data. Similarly, the laboratory energy of 72.2 MeV for the ^{11}B-induced reactions[9] would correspond to a bombarding energy of 118 MeV for the ^{16}O-induced reactions. As can be seen in Tables VIII and X the normalization factors required to bring the DWBA calculations of Refs. 11 and 9 into agreement with the data for reasonable spectroscopic factors are quite close to unity. With the exception of the (^{11}B, ^{10}Be) reaction these factors are within 20% of those found necessary in the present study at the corresponding ^{16}O bombarding energies (obtained by interpolation between the normalization factors for 104, 138.5, and 216.6 MeV given in Tables VIII and X).

Low and Tamura[10,13] have given a DWBA analysis of our 104- and 138.5-MeV data on the reaction ^{208}Pb(^{16}O, ^{15}N)^{209}Bi. They obtain angular distributions and relative transition rates very similar to those reported here. Low and Tamura, however, quote extracted spectroscopic factors for ^{209}Bi around unity—implying a roughly correct overall normalization, whereas our results, presented in Fig. 4, indicate DWBA cross sections too small by a factor between 1.5 and 2. This difference in normalization is a result of three relatively minor effects, all of which influence the cross sections in the same direction. First, Low and Tamura did not include Coulomb and core-Coulomb terms in the DWBA effective interaction. The additional terms reduce cross sections by about 25% for proton-transfer reactions. Second, an optical potential was used which does not yield the best fit to the elastic data. The potentials used in this study again reduce cross sections by about 25%. Finally, Low and Tamura's spectroscopic factors are roughly 25% larger than those on which our Fig. 4 is based. Use of our smaller spectroscopic factors (average $S \sim 0.7$ instead of 0.9 to 1)

reduces cross sections by another 25%. The product of these three 25% reduction factors accounts for the difference in absolute normalization between Low and Tamura and the present study.

Inspection of Table IV of Low and Tamura[10] with the hindsight provided by the new higher energy data reveals that the absolute spectroscopic factors extracted from the 138.5-MeV data are systematically about 30% smaller than those obtained from the 104-MeV data. This implies an energy dependence in the ratio $\sigma(\text{exp})/\sigma(\text{DWBA})$ somewhat smaller than, but in the same direction as, that obtained in Fig. 17. In view of the uncertainties in the DWBA analyses, it would be impossible to draw any convincing conclusions about the energy dependence from the 104- and 138.5-MeV data alone; the results of Low and Tamura, however, are not inconsistent with our conclusions about the energy dependence of DWBA.

VIII. CONCLUSIONS

Elastic scattering of ^{16}O on ^{208}Pb and the single-nucleon transfer reactions $^{208}\text{Pb}(^{16}\text{O},^{15}\text{N})^{209}\text{Bi}$ and $^{208}\text{Pb}(^{16}\text{O},^{17}\text{O})^{207}\text{Pb}$ have been measured at bombarding energies of 104, 138.5, and 216.6 MeV. These results have been used, together with data from other measurements of elastic scattering at various energies from 80 to 192 MeV and of the $(^{16}\text{O},^{15}\text{N})$ reaction at the subbarrier energy of 69.1 MeV, in a detailed optical-model-DWBA analysis.

Many features of the transfer cross sections are well reproduced by the DWBA calculations. The calculated shapes of the angular distributions are generally in good agreement with experiment; however, small systematic differences are found between calculated and observed peak angles. These angle shifts may be due to coupling to inelastic channels but no definite conclusions can be drawn until calculations are performed over a wide energy range.

The DWBA calculations reproduce the relative intensities of transitions to the different single-particle and single-hole states at each bombarding energy. This is particularly impressive since the relative intensities change rather dramatically with bombarding energy from dominance by spin-flip transitions near the Coulomb barrier to dominance by no-spin-flip transitions at higher energies. The relative spectroscopic factors used are in satisfactory accord with those obtained in previous studies with both light and heavy ions.

The measured energy dependence of the single-nucleon transfer reactions is found to be much less rapid than is predicted by DWBA. This discrepancy is insensitive to variations in the form factor (within the limits of the spherical single-particle shell model) and to variations in the optical-model parameters (within the limits of the conventional local, L-independent Woods-Saxon form) provided that a reasonable fit is maintained to the elastic data at all energies. The rapid decrease of $\sigma(\text{exp})/\sigma(\text{DWBA})$ with increasing energy has been confirmed in recent measurements[5,6] at 312.6 MeV. It is clear that a conventional optical-model-DWBA analysis of the single-nucleon transfer reactions induced by ^{16}O on ^{208}Pb is in gross disagreement with experiment; it amounts to factors from 4 to 8 between the Coulomb barrier and 312.6 MeV.

Three possible ways of accounting for this discrepancy, polarization of the shell-model orbitals, coupled-channel calculations (with a few active channels), and the use of less-restricted forms of optical-model potentials, are discussed in Sec. VI. The discrepancy is so large that it is difficult to imagine any one of these approaches sufficing in itself to remove the disagreement between theory and experiment.

Our work points to the importance of detailed measurements of elastic scattering, transfer, and fusion cross sections in the region from 110 to 170 MeV. In particular it would be of interest to check whether or not the total reaction cross section varies smoothly with energy, whether the ratio $\sigma(\text{exp})/\sigma(\text{DWBA})$ heads steadily downhill from the Coulomb barrier or whether there is a region of constancy followed by a break, and finally whether this break (if any) is correlated with the energy dependence of the fusion cross section. We believe that the discrepancy we have exhibited between the energy dependences of experimental and DWBA transfer cross sections is of great significance and that its resolution should shed light on the dynamics of heavy-ion interactions.

This work was performed under the auspices of USDOE, Division of Physical Research.

---

*Present address: Institute for Defense Analysis, 400 Army-Navy Drive, Arlington, Va. 22202.
†Present address: Argonne National Laboratory, Argonne, Illinois 60439.
‡Present address: Cyclotron Laboratory, Physics Department, University of Michigan, Ann Arbor, Michigan 48105.
§Present address: Hahn-Meitner Institute, Berlin, Germany.
||Present address: Gesellschaft für Schwerionenforschung, Darmstadt Wixhausen, Germany.

[1] F. Videbaek, R. B. Goldstein, L. Grodzins, S. G. Steadman, T. A. Belote, and J. D. Garrett, Phys. Rev. C 15, 954 (1977).

[2]J. D. Garrett, A. Z. Schwarzschild, C. E. Thorn, and W. von Oertzen, Bull. Am. Phys. Soc. 19, 1025 (1974).
[3]J. B. Ball, C. B. Fulmer, E. E. Gross, M. L. Halbert, D. C. Hensley, C. A. Ludemann, M. J. Saltmarsh, and G. R. Satchler, Nucl. Phys. A252, 208 (1975).
[4]A. R. Barnett, W. R. Phillips, P. J. A. Buttle, and L. J. B. Goldfarb, Nucl. Phys. A176, 321 (1971).
[5]D. G. Kovar, F. D. Becchetti, B. G. Harvey, F. Pühlhofer, J. Mahoney, D. W. Miller, and M. S. Zisman, Phys. Rev. Lett. 29, 1023 (1972); D. K. Scott, in *Lecture Notes in Physics*, edited by H. L. Harney, P. Braun-Munzinger, and C. K. Gelbke (Springer, New York, 1975), Vol. 33, 165.
[6]D. G. Kovar, B. G. Harvey, F. D. Becchetti, J. A. Mahoney, D. L. Hendrie, H. Homeyer, W. von Oertzen, and M. A. Nagarajan, Phys. Rev. Lett. 30, 1075 (1973).
[7]C. Olmer, M. Mermaz, M. Buenerd, C. K. Gelbke, D. L. Hendrie, J. Mahoney, A. Menchaca-Rocha, D. K. Scott, M. H. Macfarlane, and S. C. Pieper, Phys. Rev. Lett. 38, 476 (1977).
[8]K. S. Low and T. Tamura, Phys. Lett. 48B, 285 (1974).
[9]J. L. C. Ford, Jr., K. S. Toth, G. R. Satchler, D. C. Hensley, L. W. Owen, R. M. DeVries, R. M. Gaedke, P. J. Riley, and S. T. Thornton, Phys. Rev. C 10, 1429 (1974).
[10]K. S. Low and T. Tamura, Phys. Rev. C 11, 789 (1975).
[11]K. S. Toth, J. L. C. Ford, Jr., G. R. Satchler, E. E. Gross, D. C. Hensley, S. T. Thornton, and T. C. Schweizer, Phys. Rev. C 14, 1471 (1976).
[12]J. S. Larsen, J. L. C. Ford, Jr., R. M. Gaedke, K. S. Toth, J. B. Ball, and R. L. Hahn, Phys. Lett. 42B, 205 (1972).
[13]T. Tamura and K. S. Low, Phys. Rev. Lett. 31, 1356 (1973).
[14]F. D. Becchetti, B. G. Harvey, D. Kovar, J. Mahoney, C. Maguire, and D. K. Scott, Phys. Rev. C 12, 894 (1975).
[15]W. von Oertzen, in Proceedings of the Symposium on Heavy-ion Transfer Reactions, Argonne, 1973 [Argonne National Laboratory Informal Report No. PHY 1973B, 1973 (unpublished), p. 675].
[16]B. G. Harvey, J. Mahoney, F. G. Pühlhofer, F. S. Golding, D. A. Landis, J. C. Faivre, D. G. Kovar, M. S. Zisman, J. R. Meriwether, S. W. Cosper, and D. L. Hendrie, Nucl. Instrum. Methods 104, 21 (1972).
[17]See AIP document number PAPS PRVCA 18-180-4 for tabulations of the data reported in this article. Order by PAPS number and journal reference from American Institute of Physics, Physics Auxiliary Publication Service, 335 East 45th Street, New York, N.Y. 10017. The price is $1.50 for microfiche or $5.00 for a photocopy. Make checks payable to AIP. This material also appears in *Current Physics Microfilms* on the frames immediately following this journal article.
[18]J. D. Garrett, private communication.
[19]J. B. Ball, private communication.
[20]D. H. Gloeckner, M. H. Macfarlane, and S. C. Pieper, Argonne Nat. Lab. Report No. ANL-76-11, 1976 (unpublished).
[21]D. H. Gloeckner, M. H. Macfarlane, and S. C. Pieper, Comput. Phys. Commun. 11, 299 (1976).
[22]J. G. Cramer, R. M. DeVries, D. A. Goldberg, M. S. Zisman, and C. F. Maguire, Phys. Rev. C 14, 2158 (1976).
[23]G. R. Satchler, Argonne Nat. Lab. Report No. ANL/PHY-76-2, p. 33 (unpublished).
[24]C. Olmer, private communication.
[25]R. M. DeVries, G. R. Satchler, and J. G. Cramer, Phys. Rev. Lett. 32, 1377 (1974).
[26]W. Henning, Y. Eisen, J. R. Erskine, D. G. Kovar, and B. Zeidman, Phys. Rev. C 15, 292 (1977).
[27]C. J. Batty and C. N. Greenlees, Nucl. Phys. A133, 673 (1969).
[28]W. C. Parkinson, D. L. Hendrie, H. H. Duhm, J. Mahoney, J. Saudinos, and G. R. Satchler, Phys. Rev. 178, 1976 (1969).
[29]B. H. Wildenthal, B. M. Preedom, E. Newman, and M. R. Cates, Phys. Rev. Lett. 19, 960 (1967).
[30]A. M. Lane and R. G. Thomas, Rev. Mod. Phys. 30, 257 (1958).
[31]E. Rost, Phys. Lett. 26B, 184 (1968).
[32]C. J. Batty, Phys. Lett. 31B, 496 (1970).
[33]H. J. Gils and H. Rebel, Phys. Rev. C 13, 2159 (1976).
[34]S. D. Schery, D. A. Lind, and C. D. Zafiratos, Phys. Rev. C 9, 416 (1974).
[35]A. M. Bernstein and W. A. Seidler, Phys. Lett. 39B, 583 (1972).
[36]G. J. Igo, P. D. Barnes, E. R. Flynn, and D. D. Armstrong, Phys. Rev. 177, 1831 (1969).
[37]H. J. Korner and J. P. Schiffer, Phys. Rev. Lett. 27, 1457 (1971).
[38]E. Friedman, D. Nir, D. Suraqui, and Y. Tuchman, Phys. Rev. C 9, 2340 (1974).
[39]E. Friedman and C. J. Batty, Phys. Rev. C 16, 1425 (1977).
[40]L. Rosen, J. G. Beery, and A. S. Goldhaber, Ann. Phys. (N.Y.) 34, 96 (1965).
[41]A. H. Hussein, J. M. Cameron, S. T. Lam, G. C. Neilson, and J. Soukup, Phys. Rev. C 15, 233 (1977).
[42]G. R. Satchler, W. C. Parkinson, and D. L. Hendrie, Phys. Rev. 187, 1491 (1969).
[43]R. P. Singhal, J. R. Mareira, and H. S. Caplan, Phys. Rev. Lett. 24, 73 (1970).
[44]J. Sick and J. S. McCarthy, Nucl. Phys. A150, 631 (1970).
[45]W. Schatz, Z. Phys. A273, 69 (1975).
[46]R. C. Fuller and P. J. Moffa, Phys. Rev. C 15, 266 (1977).
[47]B. S. Reehal and B. H. Wildenthal, Part. Nucl. 6, 137 (1973).
[48]M. Gaillard, R. Bouché, L. Feuvrais, P. Gaillard, A. Guichard, M. Gusakow, J. L. Leonhardt, and J. R. Pizzi, Nucl. Phys. A119, 161 (1968).
[49]K. H. Purser, W. P. Alford, D. Cline, W. H. Fulbright, H. E. Gove, and M. S. Krick, Nucl. Phys. A132, 75 (1969).
[50]J. C. Hiebert, E. Newman, and R. H. Bassel, Phys. Rev. 154, 898 (1967).
[51]P. Ring and E. Werner, Nucl. Phys. A211, 198 (1973).
[52]M. D. Cooper, W. F. Hornyak, and P. G. Roos, Nucl. Phys. A218, 249 (1974).
[53]S. T. Thornton, Nucl. Phys. A137, 531 (1969).
[54]I. M. Naqib and L. L. Green, Nucl. Phys. A112, 76 (1968).
[55]C. J. Oliver, P. D. Forsyth, J. L. Hutton, G. Kaye,

and J. R. Milnes, Nucl. Phys. A127, 567 (1969).
[56]C. Olmer, M. Mermaz, M. Buenerd, C. K. Gelbke, D. L. Hendrie, J. Mahoney, D. K. Scott, M. H. Macfarlane, and S. C. Pieper, following paper, Phys. Rev. C 18, 205 (1978).
[57]K. Pruess, G. Delic, L. A. Charlton, and N. K. Glendenning, in Proceedings of the Symposium on Macroscopic Features of Heavy-Ion Collisions, Argonne Natl. Lab. Report No. ANL/PHY-76-2, 723 (unpublished), and Lawrence Berkeley Laboratory Report No. LBL-5008, 1976 (unpublished).
[58]D. G. Kovar, in *Symposium on Macroscopic Features of Heavy-ion Collisions, Hakone, Japan* (Institute of Physical and Chemical Research, 1977).
[59]M. Buenerd, C. K. Gelbke, B. G. Harvey, D. L. Hendrie, J. Mahoney, A. Menchaca-Rocha, C. Olmer, and D. K. Scott, Phys. Rev. Lett. 37, 1191 (1976).
[60]C. Ellegaard and P. Vedelsby, Phys. Lett. 26B, 155 (1968).
[61]G. R. Satchler, Phys. Rev. C 4, 1485 (1971).
[62]J. Bardwick and R. Tickle, Phys. Rev. 171, 1305 (1968).
[63]S. M. Smith, P. G. Roos, C. Moazed, and A. M. Bernstein, Nucl. Phys. A173, 32 (1971).
[64]W. A. Lanford and G. M. Crawley, Phys. Rev. C 9, 646 (1974).